
Harnessing Wireless Channels for Scalable and Privacy-Preserving Federated Learning

Anis Elgabli

Centre for Wireless Communications
University of Oulu, Finland
anis.elgabli@oulu.fi

Jihong Park

School of Information Technology
Deakin University, Australia
jihong.park@deakin.edu.au

Chaouki Ben Issaid

Centre for Wireless Communications
University of Oulu, Finland
chaouki.benissaid@oulu.fi

Mehdi Bennis

Centre for Wireless Communications
University of Oulu, Finland
mehdi.bennis@oulu.fi

Abstract

Wireless connectivity is instrumental in enabling scalable federated learning (FL), yet wireless channels bring challenges for model training, in which channel randomness perturbs each worker’s model update while multiple workers’ updates incur significant interference under limited bandwidth. To address these challenges, in this work we formulate a novel constrained optimization problem, and propose an FL framework harnessing wireless channel perturbations and interference for improving privacy, bandwidth-efficiency, and scalability. The resultant algorithm is coined *analog federated ADMM (A-FADMM)* based on analog transmissions and the alternating direct method of multipliers (ADMM). In A-FADMM, all workers upload their model updates to the parameter server (PS) using a single channel via analog transmissions, during which all models are perturbed and aggregated over-the-air. This not only saves communication bandwidth, but also hides each worker’s exact model update trajectory from any eavesdropper including the honest-but-curious PS, thereby preserving data privacy against model inversion attacks. We formally prove the convergence and privacy guarantees of A-FADMM for convex functions under time-varying channels, and numerically show the effectiveness of A-FADMM under noisy channels and stochastic non-convex functions, in terms of convergence speed and scalability, as well as communication bandwidth and energy efficiency.

1 Introduction

Wireless connectivity has a great potential to scale up federated learning (FL) [1–3] by cutting the wires between workers and their parameter server (PS) [4–12]. However, wirelessly connected workers may *interfere* with each other during their over-the-air transmissions, while competing over limited bandwidth. Most existing works avoid such interference by allocating dedicated channels to different workers [4–8], which is not scalable and requires significant amounts of bandwidth to support a large number of workers. Alternatively, taking a cue from FL operations, several recent works have proposed a method harnessing interference without separate channel allocation [9–12] as we review next.

Digital FL. As illustrated in Fig. 1(a), FL aims to minimize assuming N workers, by periodically uploading the local model θ_n of each worker and downloading a global model Θ from PS. Under

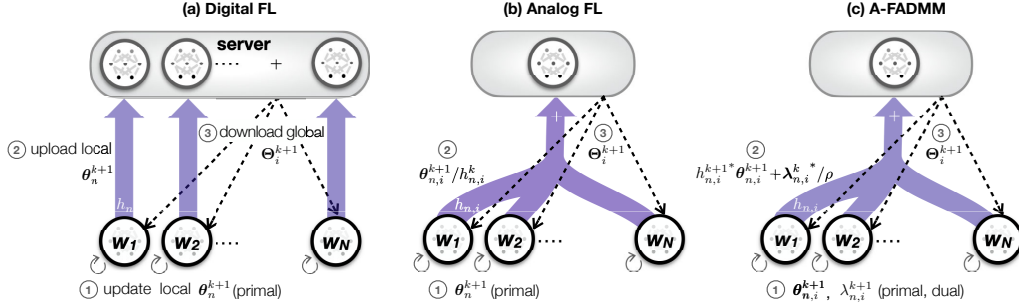


Figure 1: Schematic illustrations of: (a) digital federated learning (FL), (b) analog FL with channel inversion, and (c) *analog-federated ADMM (A-FADMM)* without channel inversion.

digital transmissions, i.e., *digital FL*, (i) PS first receives each θ_n through a *separate channel per each worker*, and (ii) combines them into a global model $\Theta = \frac{1}{N} \sum_{n=1}^N \theta_n$. The first step is however vulnerable to model inversion and reconstruction attacks [13, 14] by an honest-but-curious PS. Since the entire model update trajectory is observable, the PS can infer the training samples, violating data privacy. Furthermore, it is not communication-efficient because workers have to be assigned orthogonal channels in order for the PS to decode their models. However, the PS only needs $\sum_{n=1}^N \theta_n$ rather than individual local models, motivating the need for analog over-the-air aggregation schemes as described next.

Analog FL. Unlike digital signal transmission of bit streams, each analog signal directly represents an element $\theta_{n,i}$ of θ_n by its amplitude, allowing signal superposition. Exploiting this property, each worker in *analog FL* transmits an analog signal $\theta_{n,i}$ over a *shared channel among all workers*, through which all $\theta_{n,i}$'s are superpositioned over the air while hiding each private local model in the crowd. Consequently, the PS receives $\sum_{n=1}^N h_{n,i} \theta_{n,i}$ that is *perturbed* by complex fading channel $h_{n,i}$. Due to the perturbed models, the convergence and accuracy of analog FL depend significantly on the channel characteristics; e.g., highly dynamic channels require extremely small step sizes for guaranteeing convergence [11]. To obviate this problem, it is common to cancel out the perturbation via a *channel inversion* method dividing $\theta_{n,i}$ by $h_{n,i}$ before transmissions, as illustrated in Fig. 1(b). With channel inversion, transmissions are only allowed when $|h_{n,i}| \geq \varepsilon$, in order to avoid excessive transmit power due to the inversion [9–11]. The choice of ε is heuristic, hindering the convergence analysis of analog FL. Moreover, this approach does not guarantee privacy. For example, when only one worker has a good gain in one channel, it reveals its local model updates to the PS, compromising privacy. These limitations mandate a non-channel inversion method with formal convergence and privacy guarantees.

Main Result – Analog Federated ADMM (A-FADMM). We propose A-FADMM, a novel federated learning framework rooted in the alternating direction method of multipliers (ADMM) and analog over-the-air aggregation without channel inversion. Compared to the existing analog FL algorithms [9–11] based on first-order methods such as GD and SGD, A-FADMM is a *second-order* method providing faster convergence [15, 16]. Furthermore, A-FADMM does not apply channel inversion, so the PS receives the aggregate of perturbed model updates, thereby preserving privacy even when a single worker is transmitting over a given channel. This is done by integrating channel perturbations into the problem formulation, which may hamper the convergence particularly under time-varying channels. A-FADMM thus carefully updates model parameters so that the channel distribution changes do not hinder its convergence.

Contributions. Our major contributions are summarized as follows.

- On the theory front, this is the first work on analog transmission based distributed ADMM (primal-dual method) ensuring convergence while preserving privacy, under convex functions and time-varying channel dynamics. Existing works on analog FL focus on first-order primal methods, without proving convergence nor privacy guarantees [9–11].
- On the algorithmic front, our proposed A-FADMM is the first analog FL algorithm overcoming channel perturbations without channel inversion.

- We numerically show that A-FADMM converges faster with comparable accuracy, compared to its digital transmission counterpart D-FADMM. Our simulations clarify under which conditions A-FADMM is preferable to D-FADMM, in terms of energy-efficiency, low-latency, and scalability.
- To further support the feasibility of A-FADMM, we elaborate on how to cope with constrained transmit power. Moreover, to corroborate the feasibility under stochastic and non-convex functions, we provide simulation results for the stochastic version of A-FADMM (SA-FADMM) based on a deep neural network (DNN) in an image classification task.

2 Method

A-FADMM aims to aggregate multiple workers' updates at the PS without competition on available bandwidth via analog transmissions. In this section, we describe A-FADMM operations based on a novel problem formulation, and explain how A-FADMM copes with the nuisances incurred by analog transmissions, in terms of time-varying channel fading, noise, and transmit power limitation.

Problem Formulation. The original problem of FL is to minimize $\frac{1}{N} \sum_{n=1}^N f_n(\Theta)$ with N workers, by locally minimizing $f_n(\theta_n)$ at each worker and globally averaging their model parameters θ_n at the PS. This boils down to an average consensus problem **(P1)** on the LHS below.

$$\begin{aligned} \text{(P1)} \quad \min_{\Theta, \{\theta_n\}_{n=1}^N} \quad & \sum_{n=1}^N f_n(\theta_n) \quad (1) & \text{(P2)} \quad \min_{\Theta, \{\theta_n\}_{n=1}^N} \quad & \sum_{n=1}^N f_n(\theta_n) \quad (3) \\ \text{s.t.} \quad & \theta_n = \Theta, \quad \forall n \quad (2) & \text{s.t.} \quad & h_{n,i} \theta_{n,i} = h_{n,i} \Theta_i, \quad \forall n, i \quad (4) \end{aligned}$$

Primal-dual methods can solve **(P1)**, among which ADMM is one popular approach [15–17]. To implement this using digital transmissions, N workers transmit their local model updates to the PS through N *orthogonal channels*, wherein each local model is the primal variable θ_n while its dual variable λ_n is locally updated (see the details in Appendix A). By contrast, using analog transmissions, N workers transmit the i -th element of their updates using the same i -th subcarrier of a *single channel*¹. The benefit of analog transmissions is to aggregate all workers' updates over-the-air in one channel use, but at the cost of perturbations by channel fading $h_{n,i}$ which are assumed to follow an independent and identically distributed (IID) complex Gaussian distribution. These fading perturbations are often cancelled by multiplying $1/h_{n,i}$ before transmission, i.e., channel inversion [9–11]. Alternatively, we avoid channel inversion by reformulating **(P1)** into **(P2)** on the RHS above, where the subscript i denotes the i -th element. In **(P2)**, (2) is recast as its equivalent constraint (4) that allows A-FADMM to be updated directly using perturbed updates, as detailed next.

Primal, Dual, and Global Model Updates. The Lagrangian of **(P2)** is written as follows

$$\mathcal{L}_\rho(\theta_n, \lambda) = \sum_{n=1}^N f_n(\theta_n) + \sum_{i=1}^d \sum_{n=1}^N \lambda_{n,i}^* h_{n,i} (\theta_{n,i} - \Theta_i) + \frac{\rho}{2} \sum_{i=1}^d \sum_{n=1}^N |h_{n,i}|^2 (\theta_{n,i} - \Theta_i)^2, \quad (5)$$

where $\lambda_{n,i}^*$ is the conjugate of the complex dual variable $\lambda_{n,i}$, d is the cardinality of θ_n (i.e., model size), and $\rho > 0$ is a constant penalty for the local and global model disagreement. At iteration $k + 1$, each worker updates its primal variable θ_n^{k+1} so as to minimize $\mathcal{L}_\rho(\theta_n, \Theta^k, \lambda^k)$. Hence, $\theta_{n,i}^{k+1}$ should satisfy the following equation:

$$\text{(Primal)} \quad 0 \in \partial_i f_n(\theta_n^{k+1}) + \lambda_{n,i}^k h_{n,i} + \rho |h_{n,i}|^2 (\theta_{n,i}^{k+1} - \Theta_i^k), \quad \forall i = 1, \dots, d, \quad (6)$$

where $\partial_i f_n(\cdot)$ denotes the i -th element in the sub-gradient vector of $f_n(\cdot)$.

Next, PS updates the i -th element Θ_i^{k+1} of the global model that minimizes $\mathcal{L}_\rho(\theta_n^{k+1}, \Theta, \lambda^k)$. By taking the derivative of $\mathcal{L}_\rho(\theta_n^{k+1}, \Theta, \lambda^k)$ with respect to Θ_i and equating to zero, Θ_i^{k+1} is given by:

$$\text{(Global)} \quad \Theta_i^{k+1} = \frac{1}{\sum_{n=1}^N |h_{n,i}|^2} \sum_{n=1}^N \left(|h_{n,i}|^2 \theta_{n,i}^{k+1} + h_{n,i} \lambda_{n,i}^k / \rho \right). \quad (7)$$

¹A single channel is split into subcarriers under orthogonal frequency division multiple access (OFDMA); e.g., in 5G systems, a 50MHz channel with 15Hz carrier spacing provides 3.3k subcarriers during 10ms [18].

Algorithm 1 Analog Federated ADMM (A-FADMM)

```

1: Input:  $N, f_n(\theta_n) \forall n, \rho, K$ , Output:  $\theta_n, \forall n$ 
2: Initialization:  $\theta_n^{(0)}, \Theta_n^{(0)}, \lambda_n^{(0)}, \forall n$ 
3: A-FADMM:
4: while  $k \leq K$  do
5:   All workers ( $n \in \{1, \dots, N\}$ ): in Parallel
6:   for  $i = 1, \dots, d$  do
7:     if  $h_{n,i}^{k+1} = h_{n,i}^k$  then
8:       Find  $\theta_{n,i}^{k+1}$  that satisfies (10)
9:     else
10:       $\theta_{n,i}^{k+1} = \theta_{n,i}^k$ 
11:      Find  $(\lambda_{n,i}^k)^*$  that satisfies (10)
12:     end if
13:   end for
14:   Send  $(h_{n,i}^{k+1})^* \theta_{n,i}^{k+1} + (\lambda_{n,i}^k)^* / \rho, \forall i = 1, \dots, d$  to the parameter server
15:   Parameter Server:
16:   Find  $\Theta_i^{k+1}$  that satisfies (9)
17:   Broadcast  $\Theta_i^{k+1}, \forall i = 1, \dots, d$  to all workers
18:   All workers ( $n \in \{1, \dots, N\}$ ): in Parallel
19:     Update  $\lambda_{n,i}^{k+1}$  locally via (11)
20:    $k \leftarrow k + 1$ 
21: end while

```

Finally, the dual variables are updated at each worker as follows:

$$\text{(Dual)} \quad \lambda_{n,i}^{k+1} = \lambda_{n,i}^k + \rho h_{n,i} (\theta_{n,i}^{k+1} - \Theta_i^{k+1}). \quad (8)$$

Next, we will discuss how to implement the aforementioned update rules under time-varying channel fading, noise, and transmit power limitation.

Time-varying Channel. The primal-dual update rules in (6) and (8) do not ensure the non-increase of the optimality gap when $h_{n,i}^{k+1} \neq h_{n,i}^k$. In this case, instead of updating $\theta_{n,i}^{k+1}$ using (6), we choose $\theta_{n,i}^{k+1} = \theta_{n,i}^k$, and find $\lambda_{n,i}^k$ that satisfies (6); in other words, the primal update problem (6) is flipped to the dual update problem. In doing so, A-FADMM copes with the channel changes reflected in the dual variables, and ensures that the primal-dual variables are still optimal for the given channel $h_{n,i}^{k+1}$.

Uploading and Downloading Information. We assume that every worker knows its individual channel $h_{n,i}^{k+1}$, while the PS knows the aggregate channel $\sum_{n=1}^N |h_{n,i}^{k+1}|^2$ using pilot signals [19]. Then, to update the i -th element of the global model Θ_i , each worker uploads $h_{n,i}^{k+1*} \theta_{n,i}^{k+1} + \lambda_{n,i}^k / \rho$, where $h_{n,i}^k$ is the conjugate of the complex channel $h_{n,i}$. Hence, after channel perturbation, the PS receives $\sum_{n=1}^N (|h_{n,i}^{k+1}|^2 \theta_{n,i}^{k+1} + h_{n,i}^{k+1} \lambda_{n,i}^k / \rho)$ in (7). By downloading Θ_i , each worker locally updates the primal and dual variables using (6) and (8), respectively.

Noisy Channel. In practical systems, the received signal is not only perturbed by channel fading but also distorted by additive white Gaussian noise (AWGN). Under digital transmissions, the noise can be alleviated using digital modulation and error correction coding schemes [20, 21], while under analog transmissions, it can be mitigated by matched filtering (i.e., correlator receiver) as follows. In the uplink, each worker transmits $h_{n,i}^{k+1*} \theta_{n,i}^{k+1} + \lambda_{n,i}^k / \rho$ over the i -th subcarrier for T seconds, and the PS receives $\sum_{n=1}^N (|h_{n,i}^{k+1}|^2 \theta_{n,i}^{k+1} + h_{n,i}^{k+1} \lambda_{n,i}^k / \rho) + z_{n,i}^{k+1}(t)$ at every instant $t \in [0, T]$, where the AWGN $z_{n,i}^{k+1}(t) \sim \mathcal{CN}(0, N_o)$. The matched filter at the PS integrates the uploaded signals during T , divides by T , and takes a sample at $t = T$, resulting in $\sum_{n=1}^N (|h_{n,i}^{k+1}|^2 \theta_{n,i}^{k+1} + h_{n,i}^{k+1} \lambda_{n,i}^k / \rho) + z_{n,i}^{k+1}$ with the reduced noise $z_{n,i}^{k+1} \sim \mathcal{CN}(0, N_o/T)$. Accordingly, the global model update is given by:

$$\text{(Global)} \quad \Theta_i^{k+1} = \frac{1}{\sum_{n=1}^N |h_{n,i}^{k+1}|^2} \sum_{n=1}^N \left(|h_{n,i}^{k+1}|^2 \theta_{n,i}^{k+1} + h_{n,i}^{k+1} \lambda_{n,i}^k / \rho + \text{Re}\{z_{n,i}^{k+1}\} \right), \quad (9)$$

where $\text{Re}\{z_{n,i}^{k+1}\}$ comes from the fact that every other term in (9) including Θ_i^{k+1} is real, so taking the real part of the output will result in a global model that is perturbed by only the real part of the AWGN.

Likewise, in the downlink, the matched filter at each worker provides $h_{n,i}^{k+1} \Theta_i^{k+1} + z_{n,i}^{k+1}$. To make this output fit with the primal and dual updates, the output is multiplied by $h_{n,i}^{k+1*}$, and $|h_{n,i}^{k+1}|^2 \Theta_i^{k+1} + h_{n,i}^{k+1*} z_{n,i}^{k+1}$ is used for the following primal-dual update rules:

$$\text{(Primal)} \quad \mathbf{0} \in \partial_i f_n(\boldsymbol{\theta}_n^{k+1}) + (\boldsymbol{\lambda}_{n,i}^k)^* h_{n,i}^{k+1} + \rho |h_{n,i}^{k+1}|^2 (\boldsymbol{\theta}_n^{k+1} - \boldsymbol{\Theta}_i^k) - \rho \mathbf{Re}\{h_{n,i}^{k+1*} z_{n,i}^{k+1}\} \quad (10)$$

$$\text{(Dual)} \quad \boldsymbol{\lambda}_{n,i}^{k+1} = \boldsymbol{\lambda}_{n,i}^k + \rho h_{n,i}^{k+1} (\boldsymbol{\theta}_n^{k+1} - \boldsymbol{\Theta}_i^{k+1}) - \rho \mathbf{Re}\{z_{n,i}^{k+1}\}. \quad (11)$$

Note that digital transmission can be implemented for downlink since only the PS is transmitting and there is no competition on the available bandwidth. More details on analog and digital downlink are deferred to Appendices A and B.

Power Control. Another practical concern is each worker's transmit power limitation. In order not to violate the maximum power budget P , before transmission each worker calculates its local power scaling factor α_n^{k+1} such that $(\alpha_n^{k+1})^2 \sum_{i=1}^d |h_{n,i}^{k+1*} \boldsymbol{\theta}_n^{k+1} + \boldsymbol{\lambda}_{n,i}^k|^2 / \rho = P$, and sends α_n^{k+1} to the PS. Then, the PS determines $\alpha^{k+1} = \min\{\alpha_1^{k+1}, \dots, \alpha_N^{k+1}\}$ that is downloaded by every worker. Finally, each worker transmits $\alpha^{k+1} (h_{n,i}^{k+1*} \boldsymbol{\theta}_n^{k+1} + \boldsymbol{\lambda}_{n,i}^k / \rho)$ to the PS, and after matched filtering and dividing by α^{k+1} , the PS obtains $\sum_{n=1}^N (|h_{n,i}^{k+1}|^2 \boldsymbol{\theta}_n^{k+1} + h_{n,i}^{k+1} \boldsymbol{\lambda}_{n,i}^k / \rho) + z_{n,i}^{k+1} / \alpha^{k+1}$ for the global model update. Note that α^{k+1} and α_n^{k+1} are scalar values that can be exchanged with negligible communication overhead, e.g., through separate control signaling channels [18].

3 Convergence Analysis

In this section, we prove the optimality and convergence of A-FADMM for convex functions under noise-free but time-varying channels. The necessary and sufficient optimality conditions are the primal and dual feasibility given by

$$\boldsymbol{\theta}_n^* = \boldsymbol{\Theta}^* \quad \forall n \quad \text{and} \quad (12)$$

$$\mathbf{0} \in \partial_i f_n(\boldsymbol{\theta}_n^*) + \boldsymbol{\mu}_{n,i}^* \quad \forall n, \quad (13)$$

where the superscript $*$ denotes the value at the convergence point. The term $\boldsymbol{\mu}_{n,i} = \boldsymbol{\lambda}_{n,i}^* h_{n,i}$ is the dual variable combined with channel fading. According to (8), $\boldsymbol{\mu}_{n,i}$ is updated as follows

$$\boldsymbol{\mu}_{n,i}^{k+1} = \boldsymbol{\mu}_{n,i}^k + \rho |h_{n,i}^{k+1}|^2 \mathbf{r}_{n,i}^{k+1}, \quad (14)$$

where $\mathbf{r}_{n,i}^{k+1} = \boldsymbol{\theta}_n^{k+1} - \boldsymbol{\Theta}_i^{k+1}$ is the n -th worker's primal residual. Applying the modified dual update rule (14) to the primal update rule (6), we obtain

$$\mathbf{0} \in \partial_i f_n(\boldsymbol{\theta}_n^{k+1}) + \boldsymbol{\mu}_{n,i}^{k+1} + \mathbf{S}_{n,i}^{k+1}, \quad (15)$$

where $\mathbf{S}_{n,i}^{k+1} = \rho |h_{n,i}^{k+1}|^2 (\boldsymbol{\Theta}_i^{k+1} - \boldsymbol{\Theta}_i^k)$ is the n -th worker's dual residual. Now, we are in position to introduce our first result, Lemma 1.

Lemma 1 For the iterates $\boldsymbol{\theta}_n^{k+1}$ the optimality gap of A-FADMM, is upper and lower bounded as:

$$-\sum_{n=1}^N \sum_{i=1}^d \boldsymbol{\mu}_{n,i}^* \mathbf{r}_{n,i}^{k+1} \leq \sum_{n=1}^N [f_n(\boldsymbol{\theta}_n^{k+1}) - f_n(\boldsymbol{\theta}_n^*)] \leq -\sum_{n=1}^N \sum_{i=1}^d [\boldsymbol{\mu}_{n,i}^{k+1} \mathbf{r}_{n,i}^{k+1} - \mathbf{S}_{n,i}^{k+1} (\boldsymbol{\theta}_n^* - \boldsymbol{\theta}_n^{k+1})]. \quad (16)$$

The detailed proof is provided in Appendix C. The main idea for the proof is to utilize the optimality of the updates in (6) and (7). We derive the upper bound for the objective function optimality gap in terms of the primal and dual residuals as stated in (16). To get the lower bound in (16) in terms of the primal residual, the definition of the Lagrangian (5) is used at $\rho = 0$. The result in Lemma 1 is used to derive the main results in Theorem 1 presented next.

Theorem 1 When $f_n(\boldsymbol{\theta}_n)$ is closed, proper, and convex $\forall n$ and the Lagrangian \mathcal{L}_0 has a saddle point, under a *time-varying channel*, A-FADMM satisfies the following statements.

- The optimality gap is non-increasing, i.e.,

$$\sum_{n=1}^N \sum_{i=1}^d \left\{ \frac{1}{\rho |h_{n,i}^{k+1}|^2} [(\boldsymbol{\mu}_{n,i}^{k+1} - \boldsymbol{\mu}_{n,i}^*)^2 - (\boldsymbol{\mu}_{n,i}^k - \boldsymbol{\mu}_{n,i}^*)^2] + \rho |h_{n,i}^{k+1}|^2 [(\boldsymbol{\Theta}_i^{k+1} - \boldsymbol{\Theta}_i^*)^2 - (\boldsymbol{\Theta}_i^k - \boldsymbol{\Theta}_i^*)^2] \right\} \leq 0. \quad (17)$$

- The sum of the primal and dual residuals converges to zero as $k \rightarrow \infty$, i.e.,

$$\lim_{k \rightarrow \infty} (\rho |h_{n,i}^{k+1}|^2 \mathbf{r}_{n,i}^{k+1} + \mathbf{S}_{n,i}^{k+1}) = 0. \quad (18)$$

The detailed proof of Theorem 1 is provided in Appendix D. For the time-invariant scenario, we have the following corollary.

Corollary 1 For A-FADMM under a *time-invariant channel* where $h_{n,i}^{k+1} = h_{n,i}^k \forall k$, it holds that:

- The optimality gap converges to zero as $k \rightarrow \infty$, i.e., $\lim_{k \rightarrow \infty} \sum_{n=1}^N f_n(\boldsymbol{\theta}_n^k) = \sum_{n=1}^N f_n(\boldsymbol{\theta}^*)$; and
- Both primal and dual residuals converge to zero as $k \rightarrow \infty$, i.e., $\lim_{k \rightarrow \infty} \mathbf{r}_{n,i}^k = \lim_{k \rightarrow \infty} \mathbf{S}_{n,i}^k = \mathbf{0}$.

The proof can be found in Appendix E. The key idea is to define the Lyapunov function $V^k = \sum_{n=1}^N \sum_{i=1}^d [\frac{1}{\rho |h_{n,i}|^2} (\boldsymbol{\mu}_{n,i}^k - \boldsymbol{\mu}_{n,i}^*)^2 + \rho |h_{n,i}|^2 (\boldsymbol{\Theta}_i^k - \boldsymbol{\Theta}_i^*)^2]$ and show that the difference between V^{k+1} and V^k monotonically decreases with k . This property enables proving that both primal and dual residuals converge to zero. Next, we apply Lemma 1, and prove the optimality gap goes to zero.

4 Privacy Analysis

Revealing the local model update trajectory is vulnerable to model inversion and reconstruction attacks [13, 14]. These attacks infer the statistical profiles of training samples, violating data privacy. Against such an adversarial inverse problem, we aim to preserve privacy defined as follows.

Definition 1 [22] A mechanism $M: M(X) \rightarrow Y$ is defined to be privacy preserving if the input X cannot be uniquely derived from the output Y .

We treat X as local models to be protected, and consider Y as the known information at an eavesdropper such as PS or another worker. Under digital transmissions, PS receives every local model $\boldsymbol{\theta}_n^{k+1}$, always violating privacy. Under analog FL wherein PS receives $\sum_{n=1}^N \boldsymbol{\theta}_n^{k+1}$ after channel inversion, for certain iterations when only one worker sends the local model to PS, privacy is violated.

In sharp contrast, PS in A-FADMM receives $\sum_{n=1}^N (|h_{n,i}^{k+1}|^2 \boldsymbol{\theta}_{n,i}^{k+1} + h_{n,i}^{k+1} \boldsymbol{\lambda}_{n,i}^{k*} / \rho)$. This does not violate privacy since the reception is the aggregate of fading-perturbed and dual-variable-distorted local models while $h_{n,i}^*$, $\boldsymbol{\lambda}_{n,i}^{k*}$, and N are unknown at PS. Furthermore, against any eavesdropper knowing the global model trajectory, A-FADMM preserves privacy of local model and gradient trajectories as stated in the following theorems.

Theorem 2 Unless $\boldsymbol{\Theta}_i^{k+1} = \boldsymbol{\theta}_{n,i}^{k+1}$ (i.e., before convergence), at every $k + 1$, A-FADMM preserves the privacy of each local model update $\boldsymbol{\theta}_{n,i}^{k+1}$ and gradient update $\partial f_n(\boldsymbol{\theta}_n^{k+1}) \forall n, i$.

The detailed proof is in Appendix F. Intuitively, we show that the inverse problem of an eavesdropper is to solve a set of equations at every iteration, in which the number of unknowns is larger than the number of equations. Therefore, each worker's local model or gradient cannot be uniquely derived.

Theorem 3 When $\boldsymbol{\Theta}_i^{k+1} = \boldsymbol{\theta}_{n,i}^{k+1}$ (i.e., at convergence), A-FADMM preserves the privacy of the local model trajectory $\{\boldsymbol{\theta}_{n,i}^0, \dots, \boldsymbol{\theta}_{n,i}^k\}$ and gradient trajectory $\{\partial f_n(\boldsymbol{\theta}_n^1), \dots, \partial f_n(\boldsymbol{\theta}_n^{k+1})\} \forall n, i$.

The proof is provided in Appendix G. In brief, we show that after A-FADMM convergence when all local models become identical and known to an eavesdropper, this information cannot be used to derive a unique trajectory of each worker's local model and gradient updates.

5 Experiments

To validate our theoretical foundations, we numerically evaluate the performance of A-FADMM in convex (linear regression) and non-convex (image classification using DNNs) problems.

Simulation settings. For linear regression, we use the California Housing dataset [23] consisting of 20,000 samples with 6 features, i.e., model size $d = 6$. At iteration k , loss is given as $|\sum_{n=1}^N [f(\boldsymbol{\theta}_n^k) - f(\boldsymbol{\theta}^*)]|$. For image classification, we use the MNIST dataset [24] comprising 60,000 training and 10,000 test samples, each of which represents a hand-written 0-9 digit image. In this

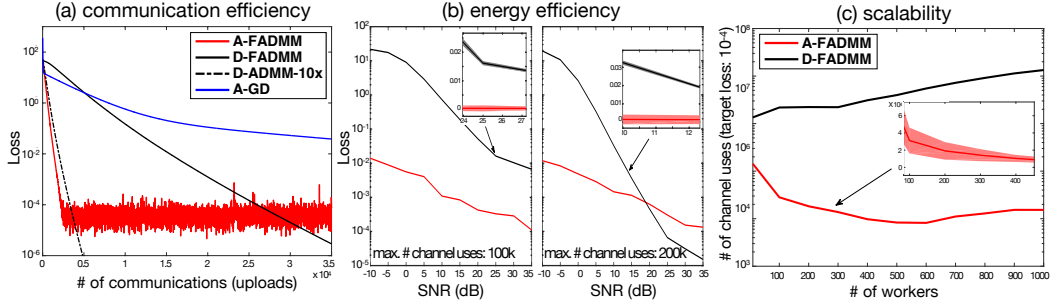


Figure 2: *Linear regression* results showing: (a) communication efficiency (loss w.r.t. # of uploads); (b) energy efficiency (loss w.r.t. SNR); and (c) scalability (# of channel uses w.r.t # of workers).

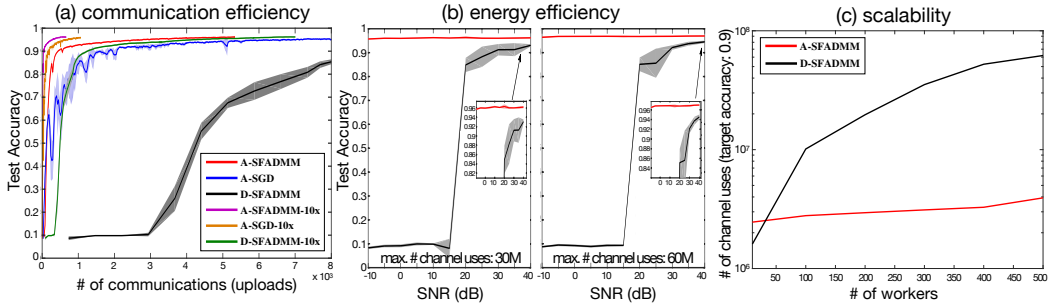


Figure 3: *Image classification* results showing: (a) communication efficiency (test accuracy w.r.t. # of uploads); (b) energy efficiency (test accuracy w.r.t. SNR); and (c) scalability (# of channel uses w.r.t # of workers).

case, we consider a 3-layer fully connected multi-layer perceptron (MLP) comprising an input layer with 784 neurons, two hidden layers with 128 and 64 neurons, respectively, and an output layer with 10 neurons, resulting in the model size $d = 109,184$. We use the rectified linear unit (ReLU) activation function, softmax output, and cross entropy loss.

By default, we consider $N = 100$ workers with $\text{SNR} = 40\text{dB}$, each of which stores the same number of training samples equally divided and allocated from the training dataset. These workers are supported using total 10 and 4,096 subcarriers for linear regression and DNNs, respectively. Following the LTE cellular standards [18], each subcarrier provides 15KHz bandwidth during 1ms. Each channel realization is coherent during 10 iterations, and is randomly generated by a Rayleigh fading distribution with zero mean and unit variance for every 10 iterations. To focus primarily on the uplink bandwidth bottleneck, we consider analog transmission only for the uplink while the downlink utilizes digital transmission (see Appendix B).

In (5), we choose the penalty constant $\rho = 0.5$ yielding fast convergence for both digital and analog implementations from our observations. To run the experiments, we use Matlab for linear regression and TensorFlow for image classification, operated in a MacBook Air computer (1.8 GHz Intel Core i5 CPU, 8 GB 1,600 MHz DDR3 RAM). For each plot, we run 5 simulations, and report mean values (solid curves) and standard deviations (shaded areas, omitted for negligible values). Finally, we compare A-FADMM with the following benchmark algorithms (optimizer details are deferred to Appendix H).

- **D-FADMM**: Digital communication version of A-FADMM, wherein the total bandwidth is equally divided and allocated to each worker whose model element consumes 32 bits
- **A-SFADMM, D-SFADMM**: Stochastic versions of A-FADMM and D-FADMM
- **A-GD, A-SGD**: Analog communication versions of the distributed gradient descent algorithm (GD), and stochastic GD algorithm (i.e., analog FL)
- **10x**: An algorithm with 10x more subcarriers than default (e.g D-FADMM-10x).

Communication Efficiency. In linear regression, as observed in Fig. 2(a), A-FADMM requires the lowest communication rounds until achieving a target loss 10^{-4} . Even with 10x more sub-

carriers, D-FADMM fails to reach the same speed due to the orthogonal subcarrier allocation to each worker under limited bandwidth. However, if one aims to achieve very low loss below 10^{-4} , A-FADMM suffers from noisy reception (see Appendix B), and D-FADMM may thus be a better choice, as long as very large bandwidth and/or long uploading time are available. In image classification, Fig.3(a) shows that A-SFADMM achieves the highest accuracy the minimum number of communication rounds. In fact, it is even more communication-efficient than D-SFADMM with 10x more subcarriers (D-SFADMM-10x).

For both tasks, analog FL (i.e., A-GD and A-SGD) struggles with intermittent uploads due to the truncated channel inversion (transmitting only when $|h_{n,i}| \geq \epsilon$). This yields too many communication rounds in linear regression (A-GD) and high variance in image classification (A-SGD), highlighting the importance of non-channel inversion methods used in A-FADMM and A-SFADMM.

Energy Efficiency vs. Accuracy. In this experiment, we assume that there are sufficient subcarriers to upload every update in one time slot, and focus on wireless communication energy consumption that often exceeds computing energy [25]. We measure loss or accuracy when the total channel uses $\sum_{i=1}^j M_i$ at time slot j reaches a target maximum number of channel uses, where M_i is the number of subcarriers used in time slot i (see the details in Appendix H).

With linear regression task and 100k maximum number of channel uses, Fig. 2(b) shows that A-FADMM always achieves order-of-magnitude lower loss than D-FADMM, even at very low -10 dB SNR, i.e., low transmit power. With 200k channel uses, D-FADMM outperforms A-FADMM, but only at high SNR exceeding 20dB. This advocates that A-FADMM is more energy-efficient and bandwidth-efficient.

In image classification, as shown by Fig. 3(b), A-SFADMM not only outperforms D-SFADMM, but also achieves the maximum test accuracy even when the SNR is as low as -10 dB and the maximum number of channel uses is 30M. By contrast, D-SFADMM with 40dB SNR and 60M channel uses achieves maximum accuracy that is still lower than A-SFADMM's.

Scalability. We investigate the scalability of A-FADMM and A-SFADMM, by counting the number of channel uses until reaching a target loss or accuracy. We vary the number of contributing workers, and we assume that the noise power spectral density is fixed as 10^{-9} W/Hz. In linear regression, we clearly see from Fig.2(c) that A-FADMM does not require more channel uses for more workers to achieve a target loss 10^{-4} . By contrast, D-FADMM necessitates the channel uses linearly proportional to the number of workers due to the orthogonal bandwidth allocation to every worker. It is worth mentioning that even with only $N = 10$ workers, A-FADMM requires order of magnitude less channel uses than D-FADMM. Similar trends are observed in Fig.3(b) for image classification, only except for the cases below $N = 10$ workers.

6 Conclusion

In this article, we proposed A-FADMM, and proved its theoretical convergence and privacy guarantees, while validating its effectiveness in convex and non-convex problems. To further improve the applicability, we conclude this article by addressing several practical issues and possible extensions.

Asynchronous Transmissions. Analog over-the-air aggregation is sensitive to asynchronous signal transmissions as both early and delayed arrivals incur additional noise at reception. To alleviate this problem, it is possible to turn the less communication rounds of A-FADMM into longer transmission time of each worker, increasing the signal overlapping duration compared to the out-of-synch duration.

Large Models. To convey large models using analog signals, model compression methods should be re-designed. Applying compressive sensing techniques is promising, in which a sparsified update is encoded by multiplying a random matrix before transmission [26], and the received update is decoded using the approximate message passing (AMP) algorithm [27].

Decentralized Architecture. Workers have limited transmit energy, and hence faraway workers are difficult to reach PS [28], hindering the wide-area coverage of A-FADMM. It could be therefore interesting to study the decentralized version of A-FADMM in which every worker communicates only with neighbors while taking into account their time-varying network topologies.

7 Broader Impact

Our work is the first principled work to enable fast, scalable, energy-efficient, and privacy-preserving model training over intermittent and time-varying wireless channels. Sitting at the intersection of two technological revolutions (5G communication and machine learning), the overarching goal of this work is to emphasize the importance of the communication and machine learning co-design, as opposed to treating them separately. Moreover, the results obtained in this work not only enable us to overcome the bottleneck of resource dimensionality in terms of timeslots and bandwidth resources, but also provide privacy-guarantees.

References

- [1] H. Brendan McMahan, Eider Moore, Daniel Ramage, et al. Communication-efficient learning of deep networks from decentralized data. In *Proceedings of Artificial Intelligence and Statistics, Fort Lauderdale, FL, USA*, April 2017.
- [2] J. Konecny, H. B. McMahan, F. X. Yu, P. Richtarik, A. T. Suresh, and D. Bacon. Federated learning: strategies for improving communication efficiency. In *Proc. of NIPS Wksp. PMPML*, Barcelona, Spain, December 2016.
- [3] Peter Kairouz, H. Brendan McMahan, Brendan Avent, Aurélien Bellet, Mehdi Bennis, et al. Advances and open problems in federated learning. *arXiv preprint arXiv:1912.04977*, 2019.
- [4] Jihong Park, Sumudu Samarakoon, Mehdi Bennis, and Mérouane Debbah. Wireless network intelligence at the edge. *to appear in Proceedings of the IEEE [Online]. Early access is available at: <https://ieeexplore.ieee.org/document/8865093>*, November 2019.
- [5] Takayuki Nishio and Ryo Yonetani. Client selection for federated learning with heterogeneous resources in mobile edge. In *Proc. Int'l Conf. Commun. (ICC), Shanghai, China*, May 2019.
- [6] S. Wang, T. Tuor, T. Salonidis, K. K. Leung, C. Makaya, T. He, and K. Chan. Adaptive federated learning in resource constrained edge computing systems. *IEEE Journal on Selected Areas in Communications*, 37(6):1205–1221, June 2019.
- [7] Howard H. Yang, Zuozhu Liu, Tony Q. S. Quek, and H. Vincent Poor. Scheduling policies for federated learning in wireless networks. *arXiv preprint arXiv: 1908.06287*, 2019.
- [8] Mingzhe Chen, Zhaohui Yang, Walid Saad, Changchuan Yin, H. Vincent Poor, and Shuguang Cui. A joint learning and communications framework for federated learning over wireless networks. *arXiv preprint arXiv: 1909.07972*, 2019.
- [9] Mohammad Mohammadi Amiri and Deniz Gunduz. Over-the-air machine learning at the wireless edge. *Proc. IEEE International Workshop on Signal Processing Advances in Wireless Communications (SP-WAC), Cannes, France*, July 2019.
- [10] Guangxu Zhu, Yong Wang, and Kaibin Huang. Broadband analog aggregation for low-latency federated edge learning. *arXiv preprint arXiv: 1812.11494*.
- [11] Tomer Sery and Kobi Cohen. On analog gradient descent learning over multiple access fading channels. *arXiv preprint arXiv: 1908.07463*.
- [12] Guangxu Zhu, Yuqing Du, Deniz Dunduz, and Kaibin Huang. One-bit over-the-air aggregation for communication-efficient federated edge learning: Design and convergence analysis. *arXiv preprint arXiv: 2001.05713*.
- [13] Matt Fredrikson, Somesh Jha, and Thomas Ristenpart. Model inversion attacks that exploit confidence information and basic countermeasures. In *Proceedings of the 22nd ACM SIGSAC Conference on Computer and Communications Security, CCS '15*, pages 1322–1333, New York, NY, USA, 2015. Association for Computing Machinery.
- [14] Briland Hitaj, Giuseppe Ateniese, and Fernando Perez-Cruz. Deep models under the gan: Information leakage from collaborative deep learning. In *Proceedings of the 2017 ACM SIGSAC Conference on Computer and Communications Security, CCS '17*, pages 603–618, New York, NY, USA, 2017. Association for Computing Machinery.
- [15] Stephen Boyd, Neal Parikh, Eric Chu, Borja Peleato, Jonathan Eckstein, et al. Distributed optimization and statistical learning via the alternating direction method of multipliers. *Foundations and Trends® in Machine learning*, 3(1):1–122, 2011.
- [16] Wei Deng, Ming-Jun Lai, Zhimin Peng, and Wotao Yin. Parallel multi-block admm with $o(1/k)$ convergence. *Journal of Scientific Computing*, 71(2):712–736, 2017.

- [17] Roland Glowinski and A Marroco. Sur l'approximation, par éléments finis d'ordre un, et la résolution, par pénalisation-dualité d'une classe de problèmes de dirichlet non linéaires. *ESAIM: Mathematical Modelling and Numerical Analysis-Modélisation Mathématique et Analyse Numérique*, 9(R2):41–76, 1975.
- [18] 3GPP. Ts 38.211 v15.2.0 release 15tr 38.802 v14.1.0. *tech. rep.*, June 2017.
- [19] M. K. Ozdemir and H. Arslan. Channel estimation for wireless ofdm systems. *IEEE Communications Surveys Tutorials*, 9(2):18–48, 2007.
- [20] Qingwen Liu, Shengli Zhou, and G. B. Giannakis. Cross-layer combining of adaptive modulation and coding with truncated arq over wireless links. *IEEE Transactions on Wireless Communications*, 3(5):1746–1755, 2004.
- [21] S. Catreux, V. Erceg, D. Gesbert, and R. W. Heath. Adaptive modulation and mimo coding for broadband wireless data networks. *IEEE Communications Magazine*, 40(6):108–115, 2002.
- [22] Chunlei Zhang, Muaz Ahmad, and Yongqiang Wang. Admm based privacy-preserving decentralized optimization. *IEEE Transactions on Information Forensics and Security*, 14(3):565–580, 2018.
- [23] Luis Torgo. Regression datasets, 2014.
- [24] Yann LeCun and Corinna Cortes. MNIST handwritten digit database. 2010.
- [25] M. S. Elbamby, C. Perfecto, C. Liu, J. Park, S. Samarakoon, X. Chen, and M. Bennis. Wireless edge computing with latency and reliability guarantees. *Proceedings of the IEEE*, 107(8):1717–1737, Aug 2019.
- [26] Mohammad Mohammadi Amiri and Deniz Gündüz. Federated learning over wireless fading channels. *arXiv preprint arXiv: 1907.09769*, 2019.
- [27] David L. Donoho, Arian Maleki, and Andrea Montanari. Message-passing algorithms for compressed sensing. *Proceedings of the National Academy of Sciences*, 106(45):18914–18919, 2009.
- [28] Anis Elgabli, Jihong Park, Amrit S Bedi, Mehdi Bennis, and Vaneet Aggarwal. GADMM: Fast and communication efficient framework for distributed machine learning. *Journal of Machine Learning Research (JMLR)*, 21(76):1–39, 2020.
- [29] D. N. C. Tse and P. Viswanath. *Fundamentals of Wireless Communications*. Cambridge University Press, 2005.

Supplementary Materials for “Harnessing Wireless Channels for Scalable and Privacy-Preserving Federated Learning”

A D-FADMM: Federated ADMM via Digital Communication

In this work, we proposed A-FADMM solving (P2) based on analog transmission. For comparison, we consider its digital transmission counterpart, D-FADMM, as elaborated next. D-FADMM solves (P1) using the standard ADMM based techniques [15–17]. Concretely, the augmented Lagrangian of (P1) is written as

$$\mathcal{L}_\rho(\Theta, \{\theta_n\}_{n=1}^N, \{\lambda_n\}_{n=1}^N) = \sum_{n=1}^N f_n(\theta_n) + \sum_{n=1}^N \langle \lambda_n, \theta_n - \Theta \rangle + \frac{\rho}{2} \sum_{n=1}^N \|\theta_n - \Theta\|_2^2, \quad (19)$$

where $\rho > 0$ is a constant penalty for the disagreement between θ_n and Θ . At iteration $k + 1$, each worker updates its primal variable by solving the following problem:

$$\text{(Primal)} \quad \theta_n^{k+1} = \arg \min_{\theta_n} \left\{ f_n(\theta_n) + \langle \lambda_n^k, \theta_n - \Theta^k \rangle + \frac{\rho}{2} \|\theta_n - \Theta^k\|_2^2 \right\}. \quad (20)$$

Based on all workers’ primal variable updates $\{\theta_n^{k+1}\}_{n=1}^N$ and previous dual variables $\{\lambda_n^k\}_{n=1}^N$, PS updates the global model Θ^{k+1} as follows:

$$\text{(Global)} \quad \Theta^{k+1} = \frac{1}{N} \sum_{n=1}^N (\theta_n^{k+1} + \frac{1}{\rho} \lambda_n^k). \quad (21)$$

Finally, given the updated global model Θ^{k+1} , each worker updates the dual variable λ_n^{k+1} as follows:

$$\text{(Dual)} \quad \lambda_n^{k+1} = \lambda_n^k + \rho(\theta_n^{k+1} - \Theta^{k+1}). \quad (22)$$

To implement the said D-FADMM operations, each worker uploads $\theta_n^{k+1} + \lambda_n^k/\rho$ to PS, and then downloads Θ^{k+1} from PS, followed by locally updating the dual variable λ^{k+1} .

Under digital transmission, the entire bandwidth is equally and orthogonally allocated to each worker, while each update uploading or downloading corresponds to exchanging a fixed number of bits, e.g., 32 bits per model’s element in our experiments in Sec. 5. The transmission and reception operations under channel noise are detailed in Appendix B. Specific parameters of the communication environments are detailed in Appendix H.

B A-FADMM and D-FADMM Under Noisy Channel

Wireless communication channels not only experience fading (mainly due to multiple propagating paths) but also additive noise (e.g., thermal noise at reception). Under digital transmission, the noise can be alleviated using digital modulation and error correction coding schemes [20, 21], while under analog transmission, matched filtering can be used as elaborated next.

D-FADMM under Channel Noise The digital communication of D-FADMM copes with channel fading and noise using adaptive modulation and error-correction coding. Therefore, the primal and dual update rules and their communicating information are the same as the procedures addressed in Appendix A.

To be precise, we describe how each update transmission can be decoded without errors in digital communication as follows. Under digital transmission, a transmitter (worker or PS) at time t encodes each update information as $x(t)$ with a code rate $R(t)$ bits/sec. The encoded bits are transmitted to a receiver (PS or worker) that receives $y(t) = h(t)x(t) + \hat{z}(t)$ where $\hat{z}(t)$ is the additive white Gaussian noise (AWGN) having zero mean and variance $N_o W$, and W Hz is the bandwidth of the subcarriers allocated to the transmitter. The variable $h(t)$ is given by a Rayleigh fading distribution with zero mean and unit variance. The received signal $y(t)$ can be successfully decoded as $x(t)$ as long as the wireless channel capacity $C(t)$ is no smaller than the code rate $R(t)$, i.e., $C(t) \geq R(t)$. Following

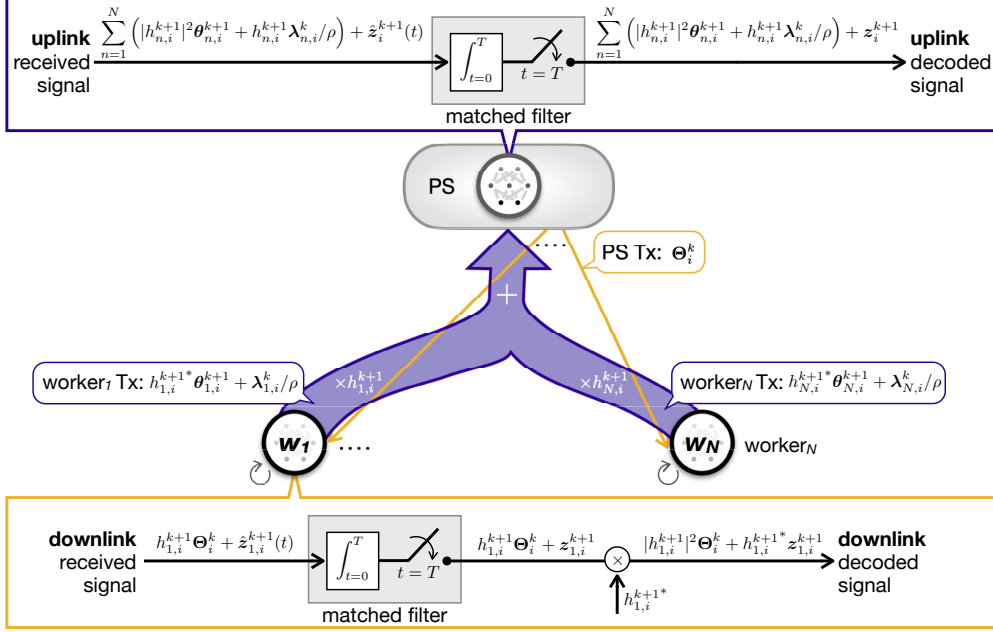


Figure 4: An illustration of uplink and downlink communication in A-FADMM under channel noise.

the Shannon formula [29], channel capacity is a function of the signal-to-noise ratio (SNR) and the subcarrier allocation, given as $C(t) = W \log_2(1 + \text{SNR}(t))$ where $\text{SNR}(t) = P|h(t)|^2/(N_oW)$. Since the channel information (i.e., $\text{SNR}(t)$) is assumed to be known before transmission using pilot signals [19], the transmitter can adjust the code rate $R(t)$ via the adaptive modulation and coding scheme (AMC) [20,21] so that $C(t) = R(t)$. Consequently, the transmitter can send its update with the rate $R(t)$ bits/sec while ensuring its error-free decoding.

A-FADMM under Noisy Channel Unlike the digital transmission of D-FADMM, the analog transmission of A-FADMM conveys uncoded information. Therefore, the received information is perturbed by multiplicative fading and distorted by additive noise. A-FADMM directly utilizes the fading perturbed updates, yet still corrects channel noise using matched filtering as follows.

As illustrated in Fig. 4, in the uplink of iteration $k + 1$, every worker in A-FADMM uploads its update $h_{n,i}^{k+1*} \theta_{n,i}^{k+1} + \lambda_{n,i}^k / \rho$ to the PS for T seconds. Propagating through the wireless channel, each update is perturbed by fading (i.e., multiplying by $h_{n,i}^{k+1}$), aggregated across all workers, and distorted by channel noise (i.e., adding $\hat{z}_i^{k+1}(t) \sim \mathcal{CN}(0, N_o)$). Consequently, the PS receives $\sum_{n=1}^N (|h_{n,i}^{k+1}|^2 \theta_{n,i}^{k+1} + h_{n,i}^{k+1} \lambda_{n,i}^k / \rho) + \hat{z}_i^{k+1}(t)$ at every instant $t \in [0, T]$. The matched filter (i.e., correlator receiver) at PS integrates the received signals during T , and takes a sample at $t = T$, resulting in

$$\frac{1}{T} \int_{t=0}^T \left\{ \left(\sum_{n=1}^N |h_{n,i}^{k+1}|^2 \theta_{n,i}^{k+1} + \lambda_{n,i}^k h_{n,i}^{k+1*} / \rho \right) + \hat{z}_i^{k+1}(t) \right\} dt = \sum_{n=1}^N |h_{n,i}^{k+1}|^2 \theta_{n,i}^{k+1} + \lambda_{n,i}^k h_{n,i}^{k+1*} / \rho + z_{n,i}^{k+1}, \quad (23)$$

where the resultant noise $z_{n,i}^{k+1} \sim \mathcal{CN}(0, N_o/T)$ whose variance is reduced from N_o to N_o/T .

Accordingly, the global model update is given by:

$$\text{(Global)} \quad \Theta_i^{k+1} = \text{Re} \left\{ \frac{1}{\sum_{n=1}^N |h_{n,i}^{k+1}|^2} \sum_{n=1}^N \left(|h_{n,i}^{k+1}|^2 \theta_{n,i}^{k+1} + h_{n,i}^{k+1} \lambda_{n,i}^k / \rho + z_{n,i}^{k+1} \right) \right\}, \quad (24)$$

where $\text{Re}\{\cdot\}$ is because Θ_i^{k+1} is real. Note that $\lambda_{n,i}^k$ is complex, but the term $h_{n,i}^{k+1} \lambda_{n,i}^k / \rho$ is still real.

Likewise, in the downlink, matched filtering at each worker yields $h_{n,i}^{k+1} \Theta_i^{k+1} + z_{n,i}^{k+1}$. To make this output fit with the primal and dual updates, the output is multiplied by $h_{n,i}^{k+1*}$, and $|h_{n,i}^{k+1}|^2 \Theta_i^{k+1} +$

$h_{n,i}^{k+1*} z_{n,i}^{k+1}$ is used for the following primal-dual update rules:

$$\text{(Primal)} \quad \mathbf{0} \in \partial_i f_n(\boldsymbol{\theta}_n^{k+1}) + (\boldsymbol{\lambda}_{n,i}^k)^* h_{n,i}^{k+1} + \rho |h_{n,i}^{k+1}|^2 (\boldsymbol{\theta}_n^{k+1} - \boldsymbol{\Theta}_i^k) - \rho \text{Re}\{h_{n,i}^{k+1*} z_{n,i}^{k+1}\} \quad (25)$$

$$\text{(Dual)} \quad \boldsymbol{\lambda}_{n,i}^{k+1} = \boldsymbol{\lambda}_{n,i}^k + \rho h_{n,i}^{k+1} (\boldsymbol{\theta}_n^{k+1} - \boldsymbol{\Theta}_i^{k+1}) - \rho \text{Re}\{z_{n,i}^{k+1}\}. \quad (26)$$

Note that to focus primarily on the uplink bandwidth bottleneck, in our experiments in Sec. 5, we consider analog transmission only for the uplink while the downlink utilizes digital transmission. Therefore, in the resultant A-FADMM implementation under channel noise, the global model update after the analog uplink reception follows (24), whereas the primal and dual updates after the digital downlink reception use the following rules:

$$\text{(Primal)} \quad \mathbf{0} \in \partial_i f_n(\boldsymbol{\theta}_n^{k+1}) + (\boldsymbol{\lambda}_{n,i}^k)^* h_{n,i}^{k+1} + \rho |h_{n,i}^{k+1}|^2 (\boldsymbol{\theta}_n^{k+1} - \boldsymbol{\Theta}_i^k) \quad (27)$$

$$\text{(Dual)} \quad \boldsymbol{\lambda}_{n,i}^{k+1} = \boldsymbol{\lambda}_{n,i}^k + \rho h_{n,i}^{k+1} (\boldsymbol{\theta}_n^{k+1} - \boldsymbol{\Theta}_i^{k+1})\}. \quad (28)$$

These noise-free primal and dual update rules are implemented as follows. In the digital downlink, each worker decodes $\boldsymbol{\Theta}_i^{k+1}$, and manually perturbs it as $|h_{n,i}^{k+1}|^2 \boldsymbol{\Theta}_i^{k+1}$ that is used for updating primal and dual variables via (27) and (28).

C Proof of Lemma 1

To prove the statement of the lemma, we will proceed by proving the following two statements

(i) The upper bound on the optimality gap is given as

$$\sum_{n=1}^N [f_n(\boldsymbol{\theta}_n^{k+1}) - f_n(\boldsymbol{\theta}_n^*)] \leq - \sum_{n=1}^N \sum_{i=1}^d \boldsymbol{\mu}_{n,i}^{k+1} \mathbf{r}_{n,i}^{k+1} + \sum_{n=1}^N \sum_{i=1}^d \mathbf{S}_{n,i}^{k+1} (\boldsymbol{\theta}_{n,i}^* - \boldsymbol{\theta}_{n,i}^{k+1}), \quad (29)$$

where $\boldsymbol{\mu}_{n,i} = \boldsymbol{\lambda}_{n,i}^* h_{n,i}$.

(ii) The lower bound on the optimality gap is given as

$$\sum_{n=1}^N [f_n(\boldsymbol{\theta}_n^{k+1}) - f_n(\boldsymbol{\theta}_n^*)] \geq - \sum_{n=1}^N \sum_{i=1}^d \boldsymbol{\mu}_{n,i}^* \mathbf{r}_{n,i}^{k+1}. \quad (30)$$

Proof of statement (i): We note that $f_n(\boldsymbol{\theta}_n)$ for all n is closed, proper, and convex, hence \mathcal{L}_ρ is sub-differentiable. Since $\boldsymbol{\theta}_n^{k+1}$ minimizes $\mathcal{L}_\rho(\boldsymbol{\theta}_n, \boldsymbol{\Theta}^k, \boldsymbol{\lambda}_n^k)$, the following must hold true at each iteration $k+1$

$$\mathbf{0} \in \partial_i f_n(\boldsymbol{\theta}_n^{k+1}) + \boldsymbol{\mu}_{n,i}^k + \rho |h_{n,i}^{k+1}|^2 \boldsymbol{\theta}_n^{k+1} - \rho |h_{n,i}^{k+1}|^2 \boldsymbol{\Theta}_i^k. \quad (31)$$

Note that when $h_{n,i}^{k+1} \neq h_{n,i}^k$, we choose $\boldsymbol{\theta}_n^{k+1} = \boldsymbol{\theta}_{n,i}^k$, and under this choice, $\boldsymbol{\theta}_n^{k+1}$ is still the minimizer of $\mathcal{L}_\rho(\boldsymbol{\theta}_n, \boldsymbol{\Theta}^k, \boldsymbol{\lambda}_n^k)$ since $\boldsymbol{\lambda}_{n,i}^k$ should have been calculated to satisfy (31) given $\boldsymbol{\theta}_{n,i}^k$ when there is change in the channel.

Adding and subtracting the term $\rho |h_{n,i}^{k+1}|^2 \boldsymbol{\Theta}_i^{k+1}$ and re-arranging the terms, we can write

$$\mathbf{0} \in \partial_i f_n(\boldsymbol{\theta}_n^{k+1}) + \boldsymbol{\mu}_{n,i}^k + \rho |h_{n,i}^{k+1}|^2 (\boldsymbol{\theta}_n^{k+1} - \boldsymbol{\Theta}_i^{k+1}) + \rho |h_{n,i}^{k+1}|^2 (\boldsymbol{\Theta}_i^{k+1} - \boldsymbol{\Theta}_i^k). \quad (32)$$

Using the definitions of $\mathbf{r}_{n,i}^{k+1}$ and $\mathbf{S}_{n,i}^{k+1}$ as well as the update of $\boldsymbol{\mu}_{n,i}^{k+1}$ given in Eq. (14), we obtain

$$\mathbf{0} \in \partial_i f_n(\boldsymbol{\theta}_n^{k+1}) + \boldsymbol{\mu}_{n,i}^{k+1} + \mathbf{S}_{n,i}^{k+1}. \quad (33)$$

The result in (33) implies that $\boldsymbol{\theta}_n^{k+1}$ minimizes the following convex objective function

$$f_n(\boldsymbol{\theta}_n) + \sum_{i=1}^d \boldsymbol{\mu}_{n,i}^{k+1} \boldsymbol{\theta}_{n,i} + \sum_{i=1}^d \mathbf{S}_{n,i}^{k+1} \boldsymbol{\theta}_{n,i}. \quad (34)$$

Next, since $\boldsymbol{\theta}_n^{k+1}$ is the minimizer of (34), then, it holds that

$$f_n(\boldsymbol{\theta}_n^{k+1}) + \sum_{i=1}^d \boldsymbol{\mu}_{n,i}^{k+1} \boldsymbol{\theta}_{n,i}^{k+1} + \sum_{i=1}^d \mathbf{S}_{n,i}^{k+1} \boldsymbol{\theta}_{n,i}^{k+1} \leq f_n(\boldsymbol{\theta}_n^*) + \sum_{i=1}^d \boldsymbol{\mu}_{n,i}^{k+1} \boldsymbol{\theta}_{n,i}^* + \sum_{i=1}^d \mathbf{S}_{n,i}^{k+1} \boldsymbol{\theta}_{n,i}^*, \quad (35)$$

where θ^* is the optimal value of the problem in (3)-(4). Summing over all workers yields

$$\begin{aligned} & \sum_{n=1}^N f_n(\theta_n^{k+1}) + \sum_{n=1}^N \sum_{i=1}^d \mu_{n,i}^{k+1} \theta_{n,i}^{k+1} + \sum_{n=1}^N \sum_{i=1}^d \mathbf{S}_{n,i}^{k+1} \theta_{n,i}^{k+1} \\ & \leq \sum_{n=1}^N f_n(\theta_n^*) + \sum_{n=1}^N \sum_{i=1}^d \mu_{n,i}^{k+1} \theta_{n,i}^* + \sum_{n=1}^N \sum_{i=1}^d \mathbf{S}_{n,i}^{k+1} \theta_{n,i}^* \end{aligned} \quad (36)$$

Similarly, Θ_i^{k+1} satisfies

$$0 = - \sum_{n=1}^N \mu_{n,i}^k + \rho \sum_{n=1}^N |h_{n,i}^{k+1}|^2 \Theta_i^{k+1} - \rho \sum_{n=1}^N |h_{n,i}^{k+1}|^2 \theta_{n,i}^{k+1}. \quad (37)$$

Using the update of $\mu_{n,i}^{k+1}$, we deduce that Θ_i^{k+1} minimizes $-\sum_{n=1}^N \mu_{n,i}^{k+1} \Theta_i$, and therefore, we can write

$$- \sum_{n=1}^N \mu_{n,i}^{k+1} \Theta_i^{k+1} \leq - \sum_{n=1}^N \mu_{n,i}^{k+1} \Theta_i^*. \quad (38)$$

Summing over all i yields

$$- \sum_{n=1}^N \sum_{i=1}^d \mu_{n,i}^{k+1} \Theta_i^{k+1} \leq - \sum_{n=1}^N \sum_{i=1}^d \mu_{n,i}^{k+1} \Theta_i^*. \quad (39)$$

Adding (36) and (39), we get

$$\begin{aligned} & \sum_{n=1}^N f_n(\theta_n^{k+1}) + \sum_{n=1}^N \sum_{i=1}^d \mu_{n,i}^{k+1} \theta_{n,i}^{k+1} + \sum_{n=1}^N \sum_{i=1}^d \mathbf{S}_{n,i}^{k+1} \theta_{n,i}^{k+1} - \sum_{n=1}^N \sum_{i=1}^d \mu_{n,i}^{k+1} \Theta_i^{k+1} \\ & \leq \sum_{n=1}^N f_n(\theta_n^*) + \sum_{n=1}^N \sum_{i=1}^d \mu_{n,i}^{k+1} \theta_{n,i}^* + \sum_{n=1}^N \sum_{i=1}^d \mathbf{S}_{n,i}^{k+1} \theta_{n,i}^* - \sum_{n=1}^N \sum_{i=1}^d \mu_{n,i}^{k+1} \Theta_i^*. \end{aligned} \quad (40)$$

After rearranging the terms, we get

$$\begin{aligned} & \sum_{n=1}^N [f_n(\theta_n^{k+1}) - f_n(\theta_n^*)] \\ & \leq - \sum_{n=1}^N \sum_{i=1}^d \mu_{n,i}^{k+1} (\theta_{n,i}^{k+1} - \Theta_i^{k+1}) + \sum_{n=1}^N \sum_{i=1}^d \mu_{n,i}^{k+1} (\theta_{n,i}^* - \Theta_i^*) + \sum_{n=1}^N \sum_{i=1}^d \mathbf{S}_{n,i}^{k+1} (\theta_{n,i}^* - \theta_{n,i}^{k+1}). \end{aligned} \quad (41)$$

Using $\mathbf{r}_{n,i}^{k+1} = \theta_{n,i}^{k+1} - \Theta_i^{k+1}$, and $\mathbf{r}_{n,i}^* = \theta_{n,i}^* - \Theta_i^* = 0$ gives

$$\sum_{n=1}^N [f_n(\theta_n^{k+1}) - f_n(\theta_n^*)] \leq - \sum_{n=1}^N \sum_{i=1}^d \mu_{n,i}^{k+1} \mathbf{r}_{n,i}^{k+1} + \sum_{n=1}^N \sum_{i=1}^d \mathbf{S}_{n,i}^{k+1} (\theta_{n,i}^* - \theta_{n,i}^{k+1}). \quad (42)$$

and hence we have proved the statement (i).

Proof of statement (ii):

We note that for a saddle point $(\Theta^*, \theta^*, \{\lambda_n^*\}_n)$ of $\mathcal{L}_0(\Theta^*, \{\theta_n\}_n, \{\lambda_n\}_n)$, it holds that, for all n , we have

$$\mathcal{L}_0(\Theta^*, \theta^*, \{\lambda_n^*\}_n) \leq \mathcal{L}_0(\Theta^{k+1}, \{\theta_n^{k+1}\}_n, \{\lambda_n^*\}_n). \quad (43)$$

Substituting the expression for the Lagrangian from (5) on the both sides of (43), we get

$$\sum_{n=1}^N f_n(\theta^*) + \sum_{n=1}^N \sum_{i=1}^d \mu_{n,i}^* (\theta_{n,i}^* - \Theta_i^*) \leq \sum_{n=1}^N f_n(\theta_n^{k+1}) + \sum_{n=1}^N \sum_{i=1}^d \mu_{n,i}^* (\theta_{n,i}^{k+1} - \Theta_i^{k+1}). \quad (44)$$

Using $\mathbf{r}_{n,i}^{k+1} = \boldsymbol{\theta}_{n,i}^{k+1} - \boldsymbol{\Theta}_i^{k+1}$, and $\mathbf{r}_{n,i}^* = \boldsymbol{\theta}_{n,i}^* - \boldsymbol{\Theta}_i^* = 0$ gives

$$\sum_{n=1}^N [f_n(\boldsymbol{\theta}_n^{k+1}) - f_n(\boldsymbol{\theta}^*)] \geq - \sum_{n=1}^N \sum_{i=1}^d \boldsymbol{\mu}_{n,i}^* \mathbf{r}_{n,i}^{k+1}. \quad (45)$$

which proves the statement (ii).

Finally, combining the statements (i) and (ii) completes the proof. \blacksquare

D Proof of Theorem 1

The proof relies on using the lower and upper bounds derived in Lemma 1 to show the decrease in the optimality gap. To this end, we start by multiplying both Eqs. (42) and (45) by 2, and then add them up to get

$$2 \sum_{n=1}^N \sum_{i=1}^d (\boldsymbol{\mu}_{n,i}^{k+1} - \boldsymbol{\mu}_{n,i}^*) \mathbf{r}_{n,i}^{k+1} + 2 \sum_{n=1}^N \sum_{i=1}^d \mathcal{S}_{n,i}^{k+1} (\boldsymbol{\theta}_{n,i}^{k+1} - \boldsymbol{\theta}_{n,i}^*) \leq 0 \quad (46)$$

Since $\boldsymbol{\mu}_{n,i}^{k+1} = \boldsymbol{\mu}_{n,i}^k + \rho |h_{n,i}^{k+1}|^2 \mathbf{r}_{n,i}^{k+1}$, then the first term can be re-written as

$$\begin{aligned} & 2 \sum_{n=1}^N \sum_{i=1}^d (\boldsymbol{\mu}_{n,i}^{k+1} - \boldsymbol{\mu}_{n,i}^*) \mathbf{r}_{n,i}^{k+1} \\ &= 2 \sum_{n=1}^N \sum_{i=1}^d (\boldsymbol{\mu}_{n,i}^k - \boldsymbol{\mu}_{n,i}^*) \mathbf{r}_{n,i}^{k+1} + 2\rho \sum_{n=1}^N \sum_{i=1}^d |h_{n,i}^{k+1}|^2 (\mathbf{r}_{n,i}^{k+1})^2. \end{aligned} \quad (47)$$

Since $\mathbf{r}_{n,i}^{k+1} = \frac{1}{\rho |h_{n,i}^{k+1}|^2} (\boldsymbol{\mu}_{n,i}^{k+1} - \boldsymbol{\mu}_{n,i}^k)$, we can write

$$\begin{aligned} & 2 \sum_{n=1}^N \sum_{i=1}^d (\boldsymbol{\mu}_{n,i}^{k+1} - \boldsymbol{\mu}_{n,i}^*) \mathbf{r}_{n,i}^{k+1} \\ &= \frac{2}{\rho} \sum_{n=1}^N \sum_{i=1}^d \frac{1}{|h_{n,i}^{k+1}|^2} (\boldsymbol{\mu}_{n,i}^k - \boldsymbol{\mu}_{n,i}^*) (\boldsymbol{\mu}_{n,i}^{k+1} - \boldsymbol{\mu}_{n,i}^k) + 2\rho \sum_{n=1}^N \sum_{i=1}^d |h_{n,i}^{k+1}|^2 (\mathbf{r}_{n,i}^{k+1})^2. \end{aligned} \quad (48)$$

Using the fact that $\boldsymbol{\mu}_{n,i}^{k+1} - \boldsymbol{\mu}_{n,i}^k = \boldsymbol{\mu}_{n,i}^{k+1} - \boldsymbol{\mu}_{n,i}^* + \boldsymbol{\mu}_{n,i}^* - \boldsymbol{\mu}_{n,i}^k$, we get

$$\frac{1}{|h_{n,i}^{k+1}|^2} (\boldsymbol{\mu}_{n,i}^k - \boldsymbol{\mu}_{n,i}^*) (\boldsymbol{\mu}_{n,i}^{k+1} - \boldsymbol{\mu}_{n,i}^k) = \frac{1}{|h_{n,i}^{k+1}|^2} (\boldsymbol{\mu}_{n,i}^k - \boldsymbol{\mu}_{n,i}^*) (\boldsymbol{\mu}_{n,i}^{k+1} - \boldsymbol{\mu}_{n,i}^*) - \frac{(\boldsymbol{\mu}_{n,i}^k - \boldsymbol{\mu}_{n,i}^*)^2}{|h_{n,i}^{k+1}|^2}. \quad (49)$$

Now, let's re-write $\rho |h_{n,i}^{k+1}|^2 (\mathbf{r}_{n,i}^{k+1})^2$, using $\mathbf{r}_{n,i}^{k+1} = \frac{1}{\rho |h_{n,i}^{k+1}|^2} (\boldsymbol{\mu}_{n,i}^{k+1} - \boldsymbol{\mu}_{n,i}^k)$, as

$$\begin{aligned} & \rho |h_{n,i}^{k+1}|^2 (\mathbf{r}_{n,i}^{k+1})^2 \\ &= \frac{1}{\rho |h_{n,i}^{k+1}|^2} (\boldsymbol{\mu}_{n,i}^{k+1} - \boldsymbol{\mu}_{n,i}^k)^2 \\ &= \frac{1}{\rho |h_{n,i}^{k+1}|^2} (\boldsymbol{\mu}_{n,i}^{k+1} - \boldsymbol{\mu}_{n,i}^*)^2 + \frac{1}{\rho |h_{n,i}^{k+1}|^2} (\boldsymbol{\mu}_{n,i}^k - \boldsymbol{\mu}_{n,i}^*)^2 - \frac{2}{\rho |h_{n,i}^{k+1}|^2} (\boldsymbol{\mu}_{n,i}^k - \boldsymbol{\mu}_{n,i}^*) (\boldsymbol{\mu}_{n,i}^{k+1} - \boldsymbol{\mu}_{n,i}^*), \end{aligned} \quad (50)$$

where we have used that $\boldsymbol{\mu}_{n,i}^{k+1} - \boldsymbol{\mu}_{n,i}^k = \boldsymbol{\mu}_{n,i}^{k+1} - \boldsymbol{\mu}_{n,i}^* + \boldsymbol{\mu}_{n,i}^* - \boldsymbol{\mu}_{n,i}^k$. Going back to Eq. (47), we can write

$$\begin{aligned} & 2 \sum_{n=1}^N \sum_{i=1}^d (\boldsymbol{\mu}_{n,i}^{k+1} - \boldsymbol{\mu}_{n,i}^*) \mathbf{r}_{n,i}^{k+1} \\ &= \frac{1}{\rho} \sum_{n=1}^N \sum_{i=1}^d \frac{1}{|h_{n,i}^{k+1}|^2} (\boldsymbol{\mu}_{n,i}^{k+1} - \boldsymbol{\mu}_{n,i}^*)^2 - \frac{1}{\rho} \sum_{n=1}^N \sum_{i=1}^d \frac{1}{|h_{n,i}^{k+1}|^2} (\boldsymbol{\mu}_{n,i}^k - \boldsymbol{\mu}_{n,i}^*)^2 + \rho \sum_{n=1}^N \sum_{i=1}^d |h_{n,i}^{k+1}|^2 (\mathbf{r}_{n,i}^{k+1})^2. \end{aligned} \quad (51)$$

Now, let's examine the second term of Eq. (46)

$$\begin{aligned}
& 2 \sum_{n=1}^N \sum_{i=1}^d \mathbf{S}_{n,i}^{k+1} (\boldsymbol{\theta}_{n,i}^{k+1} - \boldsymbol{\theta}_{n,i}^*) \\
&= 2\rho \sum_{n=1}^N \sum_{i=1}^d |h_{n,i}^{k+1}|^2 (\boldsymbol{\Theta}_i^{k+1} - \boldsymbol{\Theta}_i^k) (\boldsymbol{\theta}_{n,i}^{k+1} - \boldsymbol{\theta}_{n,i}^*) \\
&= 2\rho \sum_{n=1}^N \sum_{i=1}^d |h_{n,i}^{k+1}|^2 (\boldsymbol{\Theta}_i^{k+1} - \boldsymbol{\Theta}_i^k) \mathbf{r}_{n,i}^{k+1} + 2\rho \sum_{n=1}^N \sum_{i=1}^d |h_{n,i}^{k+1}|^2 (\boldsymbol{\Theta}_i^{k+1} - \boldsymbol{\Theta}_i^k) (\boldsymbol{\Theta}_i^{k+1} - \boldsymbol{\theta}_{n,i}^*).
\end{aligned} \tag{52}$$

Using $\boldsymbol{\Theta}_i^{k+1} - \boldsymbol{\theta}_{n,i}^* = \boldsymbol{\Theta}_i^{k+1} - \boldsymbol{\Theta}_i^k + \boldsymbol{\Theta}_i^k - \boldsymbol{\theta}_{n,i}^*$, we can write

$$\begin{aligned}
& 2 \sum_{n=1}^N \sum_{i=1}^d \mathbf{S}_{n,i}^{k+1} (\boldsymbol{\theta}_{n,i}^{k+1} - \boldsymbol{\theta}_{n,i}^*) \\
&= 2\rho \sum_{n=1}^N \sum_{i=1}^d |h_{n,i}^{k+1}|^2 (\boldsymbol{\Theta}_i^{k+1} - \boldsymbol{\Theta}_i^k) \mathbf{r}_{n,i}^{k+1} + 2\rho \sum_{n=1}^N \sum_{i=1}^d |h_{n,i}^{k+1}|^2 (\boldsymbol{\Theta}_i^{k+1} - \boldsymbol{\Theta}_i^k)^2 \\
&\quad + 2\rho \sum_{n=1}^N \sum_{i=1}^d |h_{n,i}^{k+1}|^2 (\boldsymbol{\Theta}_i^{k+1} - \boldsymbol{\Theta}_i^k) (\boldsymbol{\Theta}_i^k - \boldsymbol{\theta}_{n,i}^*).
\end{aligned} \tag{53}$$

Since $\boldsymbol{\Theta}_i^{k+1} - \boldsymbol{\Theta}_i^k = \boldsymbol{\Theta}_i^{k+1} - \boldsymbol{\theta}_{n,i}^* + \boldsymbol{\theta}_{n,i}^* - \boldsymbol{\Theta}_i^k$, then we get

$$\begin{aligned}
& 2 \sum_{n=1}^N \sum_{i=1}^d \mathbf{S}_{n,i}^{k+1} (\boldsymbol{\theta}_{n,i}^{k+1} - \boldsymbol{\theta}_{n,i}^*) \\
&= 2\rho \sum_{n=1}^N \sum_{i=1}^d |h_{n,i}^{k+1}|^2 (\boldsymbol{\Theta}_i^{k+1} - \boldsymbol{\Theta}_i^k) \mathbf{r}_{n,i}^{k+1} + 2\rho \sum_{n=1}^N \sum_{i=1}^d |h_{n,i}^{k+1}|^2 (\boldsymbol{\Theta}_i^{k+1} - \boldsymbol{\Theta}_i^k)^2 \\
&\quad - 2\rho \sum_{n=1}^N \sum_{i=1}^d |h_{n,i}^{k+1}|^2 (\boldsymbol{\Theta}_i^k - \boldsymbol{\theta}_{n,i}^*)^2 + 2\rho \sum_{n=1}^N \sum_{i=1}^d |h_{n,i}^{k+1}|^2 (\boldsymbol{\Theta}_i^{k+1} - \boldsymbol{\theta}_{n,i}^*) (\boldsymbol{\Theta}_i^k - \boldsymbol{\theta}_{n,i}^*),
\end{aligned} \tag{54}$$

Now, let's focus the second term of Eq. (54). Using $\boldsymbol{\Theta}_i^{k+1} - \boldsymbol{\Theta}_i^k = \boldsymbol{\Theta}_i^{k+1} - \boldsymbol{\theta}_{n,i}^* + \boldsymbol{\theta}_{n,i}^* - \boldsymbol{\Theta}_i^k$, we can write

$$\begin{aligned}
& \rho \sum_{n=1}^N \sum_{i=1}^d |h_{n,i}^{k+1}|^2 (\boldsymbol{\Theta}_i^{k+1} - \boldsymbol{\Theta}_i^k)^2 \\
&= \rho \sum_{n=1}^N \sum_{i=1}^d |h_{n,i}^{k+1}|^2 (\boldsymbol{\Theta}_i^{k+1} - \boldsymbol{\theta}_{n,i}^*)^2 + \rho \sum_{n=1}^N \sum_{i=1}^d |h_{n,i}^{k+1}|^2 (\boldsymbol{\Theta}_i^k - \boldsymbol{\theta}_{n,i}^*)^2 \\
&\quad - 2\rho \sum_{n=1}^N \sum_{i=1}^d |h_{n,i}^{k+1}|^2 (\boldsymbol{\Theta}_i^{k+1} - \boldsymbol{\theta}_{n,i}^*) (\boldsymbol{\Theta}_i^k - \boldsymbol{\theta}_{n,i}^*).
\end{aligned} \tag{55}$$

Replacing the last equation into Eq. (54), we can write

$$\begin{aligned}
& 2 \sum_{n=1}^N \sum_{i=1}^d \mathbf{S}_{n,i}^{k+1} (\boldsymbol{\theta}_{n,i}^{k+1} - \boldsymbol{\theta}_{n,i}^*) \\
&= 2\rho \sum_{n=1}^N \sum_{i=1}^d |h_{n,i}^{k+1}|^2 (\boldsymbol{\Theta}_i^{k+1} - \boldsymbol{\Theta}_i^k) \mathbf{r}_{n,i}^{k+1} + \rho \sum_{n=1}^N \sum_{i=1}^d |h_{n,i}^{k+1}|^2 (\boldsymbol{\Theta}_i^{k+1} - \boldsymbol{\Theta}_i^k)^2 \\
&\quad + \rho \sum_{n=1}^N \sum_{i=1}^d |h_{n,i}^{k+1}|^2 (\boldsymbol{\Theta}_i^{k+1} - \boldsymbol{\theta}_{n,i}^*)^2 - \rho \sum_{n=1}^N \sum_{i=1}^d |h_{n,i}^{k+1}|^2 (\boldsymbol{\Theta}_i^k - \boldsymbol{\theta}_{n,i}^*)^2.
\end{aligned} \tag{56}$$

Using Eqs. (51) and (56) in (46), we get

$$\begin{aligned}
& \frac{1}{\rho} \sum_{n=1}^N \sum_{i=1}^d \frac{1}{|h_{n,i}^{k+1}|^2} (\boldsymbol{\mu}_{n,i}^{k+1} - \boldsymbol{\mu}_{n,i}^*)^2 - \frac{1}{\rho} \sum_{n=1}^N \sum_{i=1}^d \frac{1}{|h_{n,i}^{k+1}|^2} (\boldsymbol{\mu}_{n,i}^k - \boldsymbol{\mu}_{n,i}^*)^2 + \rho \sum_{n=1}^N \sum_{i=1}^d |h_{n,i}^{k+1}|^2 (\mathbf{r}_{n,i}^{k+1})^2 \\
& + 2\rho \sum_{n=1}^N \sum_{i=1}^d |h_{n,i}^{k+1}|^2 (\boldsymbol{\Theta}_i^{k+1} - \boldsymbol{\Theta}_i^k) \mathbf{r}_{n,i}^{k+1} + \rho \sum_{n=1}^N \sum_{i=1}^d |h_{n,i}^{k+1}|^2 (\boldsymbol{\Theta}_i^{k+1} - \boldsymbol{\Theta}_i^k)^2 \\
& + \rho \sum_{n=1}^N \sum_{i=1}^d |h_{n,i}^{k+1}|^2 (\boldsymbol{\Theta}_i^{k+1} - \boldsymbol{\Theta}_i^*)^2 - \rho \sum_{n=1}^N \sum_{i=1}^d |h_{n,i}^{k+1}|^2 (\boldsymbol{\Theta}_i^k - \boldsymbol{\Theta}_i^*)^2 \leq 0
\end{aligned} \tag{57}$$

Defining the sequence that measures the difference in the optimality gap between iterations $k+1$ and k as

$$\begin{aligned}
W^{k+1} &= \frac{1}{\rho} \sum_{n=1}^N \sum_{i=1}^d \frac{1}{|h_{n,i}^{k+1}|^2} (\boldsymbol{\mu}_{n,i}^{k+1} - \boldsymbol{\mu}_{n,i}^*)^2 - \frac{1}{\rho} \sum_{n=1}^N \sum_{i=1}^d \frac{1}{|h_{n,i}^{k+1}|^2} (\boldsymbol{\mu}_{n,i}^k - \boldsymbol{\mu}_{n,i}^*)^2 \\
& + \rho \sum_{n=1}^N \sum_{i=1}^d |h_{n,i}^{k+1}|^2 (\boldsymbol{\Theta}_i^{k+1} - \boldsymbol{\Theta}_i^*)^2 - \rho \sum_{n=1}^N \sum_{i=1}^d |h_{n,i}^{k+1}|^2 (\boldsymbol{\Theta}_i^k - \boldsymbol{\Theta}_i^*)^2,
\end{aligned} \tag{58}$$

then, Eq. (57) can be re-written as

$$W^{k+1} \leq -\rho \sum_{n=1}^N \sum_{i=1}^d |h_{n,i}^{k+1}|^2 (\mathbf{r}_{n,i}^{k+1} + \boldsymbol{\Theta}_i^{k+1} - \boldsymbol{\Theta}_i^k)^2. \tag{59}$$

From (59), we note that W^{k+1} is ≤ 0 since ρ is a positive constant ($\rho > 0$) and the sum square term is ≥ 0 . Hence, the optimality gap at iteration $k+1$ is non-increasing, which completes the proof. ■

E Proof of Corollary 1

Using the derivations made in Theorem 1, we can further show that, in the case of static channel, i.e. $h_{n,i}^{k+1} = h_{n,i}$, both the primal and dual residuals converge to zero, i.e. $\lim_{k \rightarrow \infty} \mathbf{r}_{n,i}^{k+1} = 0$ and $\lim_{k \rightarrow \infty} \mathbf{S}_{n,i}^{k+1} = 0$. To this end, we start defining the Lyapunov function

$$V^k = \frac{1}{\rho} \sum_{n=1}^N \sum_{i=1}^d \frac{1}{|h_{n,i}|^2} (\boldsymbol{\mu}_{n,i}^k - \boldsymbol{\mu}_{n,i}^*)^2 + \rho \sum_{n=1}^N \sum_{i=1}^d |h_{n,i}|^2 (\boldsymbol{\Theta}_i^k - \boldsymbol{\Theta}_i^*)^2. \tag{60}$$

We can re-write (59) as

$$\begin{aligned}
& V^{k+1} - V^k \\
& \leq -\rho \sum_{n=1}^N \sum_{i=1}^d |h_{n,i}|^2 (\mathbf{r}_{n,i}^{k+1})^2 - \rho \sum_{n=1}^N \sum_{i=1}^d |h_{n,i}|^2 (\boldsymbol{\Theta}_i^{k+1} - \boldsymbol{\Theta}_i^k)^2 - 2\rho \sum_{n=1}^N \sum_{i=1}^d |h_{n,i}|^2 \mathbf{r}_{n,i}^{k+1} (\boldsymbol{\Theta}_i^{k+1} - \boldsymbol{\Theta}_i^k)
\end{aligned} \tag{61}$$

Since $\boldsymbol{\Theta}_i^{k+1}$ minimizes $-\sum_{n=1}^N \boldsymbol{\mu}_{n,i}^{k+1} \boldsymbol{\Theta}_i$, and $\boldsymbol{\Theta}_i^k$ minimizes $-\sum_{n=1}^N \boldsymbol{\mu}_{n,i}^k \boldsymbol{\Theta}_i$, then, after summing over i in both sides of each equation, we can write

$$-\sum_{n=1}^N \sum_{i=1}^d \boldsymbol{\mu}_{n,i}^{k+1} \boldsymbol{\Theta}_i^{k+1} \leq -\sum_{n=1}^N \sum_{i=1}^d \boldsymbol{\mu}_{n,i}^{k+1} \boldsymbol{\Theta}_i^k, \tag{62}$$

$$-\sum_{n=1}^N \sum_{i=1}^d \boldsymbol{\mu}_{n,i}^k \boldsymbol{\Theta}_i^k \leq -\sum_{n=1}^N \sum_{i=1}^d \boldsymbol{\mu}_{n,i}^k \boldsymbol{\Theta}_i^{k+1}. \tag{63}$$

Adding Eqs. (62) and (63), we get

$$\sum_{n=1}^N \sum_{i=1}^d (\boldsymbol{\mu}_{n,i}^{k+1} - \boldsymbol{\mu}_{n,i}^k) (\boldsymbol{\Theta}_i^{k+1} - \boldsymbol{\Theta}_i^k) \geq 0. \tag{64}$$

Since $\boldsymbol{\mu}_{n,i}^{k+1} = \boldsymbol{\mu}_{n,i}^k + \rho |h_{n,i}|^2 \mathbf{r}_{n,i}^{k+1}$, then we get

$$2\rho \sum_{n=1}^N \sum_{i=1}^d |h_{n,i}|^2 (\boldsymbol{\Theta}_i^{k+1} - \boldsymbol{\Theta}_i^k) \mathbf{r}_{n,i}^{k+1} \geq 0. \quad (65)$$

Thus, using Eq. (61), and summing over the iterations from $k = 1, \dots, K$, we get

$$\begin{aligned} & \sum_{k=0}^K \left[\rho \sum_{n=1}^N \sum_{i=1}^d |h_{n,i}|^2 (\mathbf{r}_{n,i}^{k+1})^2 + \rho \sum_{n=1}^N \sum_{i=1}^d |h_{n,i}|^2 (\boldsymbol{\Theta}_i^{k+1} - \boldsymbol{\Theta}_i^k)^2 \right. \\ & \left. + 2\rho \sum_{n=1}^N \sum_{i=1}^d |h_{n,i}|^2 (\boldsymbol{\Theta}_i^{k+1} - \boldsymbol{\Theta}_i^k) \mathbf{r}_{n,i}^{k+1} \right] \leq V^0. \end{aligned} \quad (66)$$

Taking the limit as $K \rightarrow \infty$, and using the fact that the terms of the serie on the left hand-side are positive, we obtain that the primal and dual residuals goes to zero as $k \rightarrow \infty$, i.e. $\lim_{k \rightarrow \infty} \mathbf{r}_{n,i}^{k+1} = \mathbf{0}$ and $\lim_{k \rightarrow \infty} \mathbf{S}_{n,i}^{k+1} = \mathbf{0}$. Using the upper and lower bounds, (16), derived in Lemma 1 and the fact that both the primal and dual residuals goes to zero as $k \rightarrow \infty$, we get that the optimal gap also goes to zero as $k \rightarrow \infty$, i.e., $\lim_{k \rightarrow \infty} \sum_{n=1}^N f_n(\boldsymbol{\theta}_n^k) = \sum_{n=1}^N f_n(\boldsymbol{\theta}_n^*)$, finalizing the proof. ■

F Proof of Theorem 2

Since $\boldsymbol{\theta}_{n,i}^0$ and $\boldsymbol{\lambda}_{n,i}^0, \forall n \in \{1, \dots, N\}, \forall i \in \{1, \dots, d\}$, are initiated randomly, then their values cannot be revealed by the eavesdropper. For simplicity, we assume that $f_n(\boldsymbol{\theta}_n^{k+1})$ is differentiable and the system is noise free. The eavesdropper needs to solve either of the following two equations to derive $\boldsymbol{\theta}_{n,i}^1$

$$\begin{cases} \boldsymbol{\theta}_{n,i}^1 = \frac{\rho |h_{n,i}^1|^2 \boldsymbol{\Theta}_i^0 - \nabla_i f_n(\boldsymbol{\theta}_n^1) - (\boldsymbol{\lambda}_{n,i}^0)^* h_{n,i}^1}{\rho |h_{n,i}^1|^2}, & \text{if } h_{n,i}^1 = h_{n,i}^0 \\ \boldsymbol{\theta}_{n,i}^1 = \boldsymbol{\theta}_{n,i}^0, & \text{if } h_{n,i}^1 \neq h_{n,i}^0 \end{cases} \quad (67)$$

$$\boldsymbol{\theta}_{n,i}^1 = \frac{\rho \sum_{n=1}^N |h_{n,i}^1|^2 \boldsymbol{\Theta}_i^1 - \rho \sum_{m=1, m \neq n}^N |h_{m,i}^1|^2 \boldsymbol{\theta}_{m,i}^1 - \sum_{n=1}^N (\boldsymbol{\lambda}_{n,i}^0)^* h_{n,i}^1}{\rho |h_{n,i}^1|^2}. \quad (68)$$

Note that the eavesdropper knows $\boldsymbol{\Theta}_i^0$ and $\boldsymbol{\Theta}_i^1$. However, the values of $h_{n,i}^1, \boldsymbol{\lambda}_{n,i}^0, \nabla_i f_n(\boldsymbol{\theta}_n^1), \rho \sum_{m=1, m \neq n}^N |h_{m,i}^1|^2 \boldsymbol{\theta}_{m,i}^1$, and $\boldsymbol{\theta}_{n,i}^0$ are unknown. Hence, even at the absence of the noise at the receiver, the eavesdropper cannot have a unique solution for $\boldsymbol{\theta}_{n,i}^1$ and/or $\nabla_i f_n(\boldsymbol{\theta}_n^1)$ since the number of variables $V = 5$ is greater than the number of equations $E = 2$.

Writing the same equations for iterations k and $k + 1$

$$\begin{cases} \boldsymbol{\theta}_{n,i}^k = \frac{\rho |h_{n,i}^k|^2 \boldsymbol{\Theta}_i^{k-1} - \nabla_i f_n(\boldsymbol{\theta}_n^k) - (\boldsymbol{\lambda}_{n,i}^{k-1})^* h_{n,i}^k}{\rho |h_{n,i}^k|^2}, & \text{if } h_{n,i}^k = h_{n,i}^{k-1} \\ \boldsymbol{\theta}_{n,i}^k = \boldsymbol{\theta}_{n,i}^{k-1}, & \text{if } h_{n,i}^k \neq h_{n,i}^{k-1} \end{cases} \quad (69)$$

$$\boldsymbol{\theta}_{n,i}^k = \frac{\rho \sum_{n=1}^N |h_{n,i}^k|^2 \boldsymbol{\Theta}_i^k - \rho \sum_{m=1, m \neq n}^N |h_{m,i}^k|^2 \boldsymbol{\theta}_{m,i}^k - \sum_{n=1}^N (\boldsymbol{\lambda}_{n,i}^{k-1})^* h_{n,i}^k}{\rho |h_{n,i}^k|^2}. \quad (70)$$

$$\begin{cases} \boldsymbol{\theta}_{n,i}^{k+1} = \frac{\rho |h_{n,i}^{k+1}|^2 \boldsymbol{\Theta}_i^k - \nabla_i f_n(\boldsymbol{\theta}_n^{k+1}) - (\boldsymbol{\lambda}_{n,i}^k)^* h_{n,i}^{k+1}}{\rho |h_{n,i}^{k+1}|^2}, & \text{if } h_{n,i}^{k+1} = h_{n,i}^k \\ \boldsymbol{\theta}_{n,i}^{k+1} = \boldsymbol{\theta}_{n,i}^k, & \text{if } h_{n,i}^{k+1} \neq h_{n,i}^k \end{cases} \quad (71)$$

$$\boldsymbol{\theta}_{n,i}^{k+1} = \frac{\rho \sum_{n=1}^N |h_{n,i}^{k+1}|^2 \boldsymbol{\Theta}_i^{k+1} - \rho \sum_{m=1, m \neq n}^N |h_{m,i}^{k+1}|^2 \boldsymbol{\theta}_{m,i}^{k+1} - \sum_{n=1}^N (\boldsymbol{\lambda}_{n,i}^k)^* h_{n,i}^{k+1}}{\rho |h_{n,i}^{k+1}|^2}. \quad (72)$$

Similarly, the eavesdropper knows Θ_i^k and Θ_i^{k+1} . However, $h_{n,i}^{k+1}$, $\lambda_{n,i}^k$, $\nabla_i f_n(\theta_n^{k+1})$, $\rho \sum_{m=1, m \neq n}^N |h_{m,i}^{k+1}|^2 \theta_{m,i}^{k+1}$, and $\theta_{n,i}^k$ are unknown. We clearly see that if the algorithm has not converged to the optimal solution yet at iteration $k+1$, i.e., $\theta_{n,i}^{k+1} \neq \Theta_i^{k+1}$, then there is no unique inversion of $\theta_{n,i}^{k+1}$ since the number of variables is more than the number of equations. This finalizes the proof. ■

G Proof of Theorem 3

When $\theta_{n,i}^{k+1} = \Theta_i^{k+1}, \forall n, i$, we know from (72) that the following terms can be found at the PS: $\sum_{n=1}^N |h_{n,i}^{k+1}|^2 \Theta_i^{k+1}$, $\rho \sum_{m=1, m \neq n}^N |h_{m,i}^{k+1}|^2 \theta_{m,i}^{k+1}$. However, the terms $(\lambda_{n,i}^k)^* h_{n,i}^{k+1}$ and $\rho |h_{n,i}^{k+1}|^2$ cannot be found, and these two terms are needed to retrieve a unique solution for $\nabla_i f_n(\theta_n^{k+1})$ using (71). Hence, $\nabla_i f_n(\theta_n^{k+1})$ cannot be uniquely derived. From (69)-(70), we clearly see that knowing $\theta_{n,i}^{k+1}$, Θ_i^k , and Θ_i^{k-1} are not enough to find a unique solution for $\nabla_i f_n(\theta_n^k)$ and $\theta_{n,i}^k$ since all other terms in the two equations including $h_{n,i}^k$ and $\lambda_{n,i}^{k-1}$ are also unknown. Therefore, the individual model at the convergence point do not release any unique information about the updating steps of the model and the function gradient trajectory, which concludes the proof. ■

H Experimental Setting Details

To perform the experiments in Sec. 5, we consider the following datasets, model architectures, training algorithms, as well as network, communication, and simulation environments.

Datasets and Model Architectures. For linear regression, we use the California Housing dataset [23] consisting of 20,000 samples with 6 features, i.e., model size $d = 6$. Each worker's objective function is $\|Y - X\Theta_n\|_2^2$. At iteration k , loss is given as $|\sum_{n=1}^N [f(\theta_n^k) - f(\theta^*)]|$.

For image classification, we use the MNIST dataset [24] comprising 60,000 training and 10,000 test samples, each of which represents a hand-written 0-9 digit image with 28x28 pixels. In this case, we consider a 3-layer fully connected multi-layer perceptron (MLP) comprising an input layer with the dimension 784, two hidden layers with 128 and 64 neurons, and an output layer with 10 neurons, resulting in the model size $d = 109,184$. We use the rectified linear unit (ReLU) activation function for each neuron and the softmax function in the output layer. The loss function is the cross entropy defined as $-\sum_i y_i \log(y'_i)$, where y_i is the ground-truth label vector, and y'_i is the output vector of the DNN model.

Network and Communication Environments. By default, we consider $N = 100$ workers with SNR = 40dB, each of which stores the same number of training samples equally divided and allocated from the training dataset. These workers are connected to PS through total 10 and 4,096 subcarriers for linear regression and image classification using DNNs, respectively.

In A-FADMM, the i -th element of the models of all workers are uploaded using the i -th sub-carrier. In linear regression, the model size is less than the number of available subcarriers, i.e., $d = 6 < 10$, and hence A-FADMM requires only one time slot (one upload) to upload all workers' models at each iteration. In image classification where $d = 109,184$, it requires $\lceil 109,184/4,096 \rceil = 27$ time slots to uploads all workers' models per iteration.

In D-FADMM, the number of uploading time slots depends not only on the number of subcarriers but also on the channel gain of each subcarrier. To be precise, following the LTE cellular standards [18], each subcarrier provides $W_i = 15\text{KHz}$ bandwidth during 1ms. Each channel realization is coherent during 10 iterations, and is randomly generated by a Rayleigh fading distribution with zero mean and unit variance for every 10 iterations. When each model element consumes 32 bits, the n -th worker requires the uploading time slots \hat{T}_n that is the minimum T_n satisfying the following condition $\int_{t=1}^{T_n} \sum_{i=1}^{4096/N} R_{n,i}(t) dt \geq 32d$, where $R_{n,i}(t) = W_i \log_2(1 + P|h_{n,i}(t)|/(W_i N_o))$ follows from the Shannon formula [29] (see more details in Appendix B). Since each worker has independent channel realizations, to upload all workers' models to PS, it requires $\hat{T} = \max\{\hat{T}_1, \hat{T}_2, \dots, \hat{T}_N\}$ time slots.

To focus primarily on the uplink bandwidth bottleneck, in A-FADMM we consider analog transmission only for the uplink while the downlink utilizes digital transmission (see Appendix B for more detail). In D-FADMM, both uplink and downlink rely on digital transmissions (see Appendix A).

Simulation Environments. To run the experiments, we use Matlab for linear regression and TensorFlow (version 2.1.0) for image classification, operated in a MacBook Air computer (1.8 GHz Intel Core i5 CPU, 8 GB 1,600 MHz DDR3 RAM). For each plot, we run 5 simulations, and report mean values (solid curves) and standard deviations (shaded areas within +/- 3 standard deviations, omitted for negligible values in some figures).

Training Algorithms. The model training algorithms and hyperparameters are specified for A-FADMM and its benchmark schemes as follows.

(For linear regression)

- **A-FADMM** is our proposed algorithm which co-designs the ADMM optimizer with the analog communication system. We choose the disagreement penalty weight $\rho = 0.5$ in (5). For different choices of ρ , we study their impact on convergence speed and accuracy in Appendix I.
- **D-FADMM** is the digital communication version of A-FADMM, wherein the total bandwidth is equally divided and allocated to each worker whose model element consumes 32 bits. i.e., the value of each element in the model vector is transmitted using 32 bits. Following A-FADMM, we use $\rho = 0.5$.
- **A-GD** is the analog communication versions of the distributed gradient descent algorithm (GD) with channel inversion that allows the n -th worker to upload its update only when the channel gain $|h_{n,i}^k| \geq \epsilon$. We use $\epsilon = 10^{-6}$ for communication and 10^{-4} learning rate for GD operations. We observed that A-GD diverges for a larger learning rate.

(For image classification)

- **A-SFADMM** is the stochastic version of A-FADMM using DNNs. For the ADMM problem, we use $\rho = 0.5$. For the local problem at each global iteration, each worker selects a mini-batch of size 100 samples at random, and uses the Adam optimizer with 0.01 learning rate to update its local model. Per global iteration, we consider 20 local iterations. For different choices of local iterations and learning rates, we study their impact on convergence speed and accuracy in Appendix I
- **D-SFADMM** is the stochastic version of D-FADMM which are utilized in the classification problem using DNN. Following A-SFADMM, we use $\rho = 0.5$, Adam optimizer with 0.01 learning rate, mini-batch size 100, and 20 local iterations per global iteration.
- **A-SGD** is the stochastic version of A-GD with channel inversion (i.e., analog FL). Following A-GD, we use $\epsilon = 10^{-6}$ for communication. For SGD operations, we use mini-batch size 100, and choose the learning rate 0.005. Note that from our observations, A-SGD incurs high oscillation under the learning rate 0.01 used in A-SFADMM and D-SFADMM.

It is worth mentioning that from our observations, under a time-varying channel (i.e., $h_{n,i}^{k+1} \neq h_{n,i}^k$), A-SFADMM and D-SFADMM still converge without updating the dual variables using (10). Instead, they can only update the primal variables based on the current dual variables using (6). Consequently, A-SFADMM and D-SFADMM can keep updating the primal variables with low computational complexity under channel variations, which could be useful in highly dynamic channel environments wherein the channel coherence time is as low as 1 iteration.

(For both linear regression and image classification)

- **10x** implies an algorithm with 10x more subcarriers (bandwidth) than the default setting. For example, compared to A-SFADMM using 4,096 subcarriers, A-SFADMM-10x utilizes 40,960 subcarriers at each iteration. Accordingly, given the MLP model size $d = 109,184$, A-SFADMM-10x requires $\lceil 109,184/40,960 \rceil = 3$ time slots for uploading all workers' models, which is 9x less than A-SFADMM requiring $\lceil 109,184/4,096 \rceil = 27$ time slots.

Finally, we elaborate the performance metrics. In Figs. 2(a) and 3(a), the number of uploads in the x-axis follows from the uploading time slot calculations in the 'Network and Communication Environments' part of this section. In Figs. 2(b) and 3(b), SNR in the x-axis indicates the average

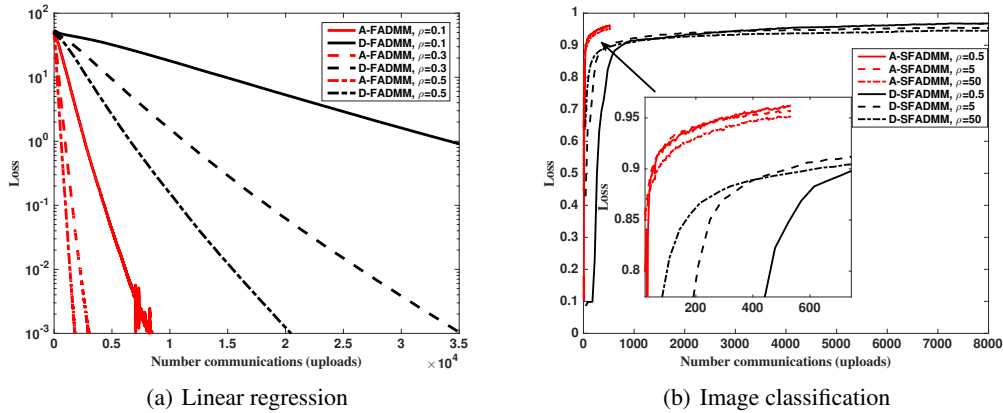


Figure 5: Impact of the *disagreement penalty weight* ρ in (a) linear regression and (b) image classification using DNNs.

SNR given as $\mathbb{E}_t[Ph_{n,i}(t)/(N_oW)] = P/(N_oW)$. In that N_oW is fixed, increasing SNR can be interpreted as increasing transmit power P . The loss or accuracy in the y-axis is measured when the total channel uses $\sum_{i=1}^j M_i$ at time slot j reaches a target maximum number of channel uses, where M_i is the number of subcarriers used in time slot i . In Figs. 2(c) and 3(c), the number of channel uses in the y-axis is calculated in the same way of the x-axis in Figs. 2(a) and 3(a), but is measured when it reaches a target loss or accuracy.

I Hyperparameter Sensitivity Analysis

In this section, we study the impact of hyperparameters on the convergence speed and accuracy of A-FADMM and D-FADMM as well as their stochastic versions. All the training, communication, and simulation environments are identical to the settings in Sec. 5 (detailed in Appendix H), except for the hyperparameters: disagreement penalty weight ρ , learning rate, and the number of local iterations as elaborated next.

Impact of ρ . The penalty weight ρ adjusts the degree of disagreement between local and global models in both linear regression and classification tasks. In linear regression, Fig. 5(a) shows that a larger ρ leads to faster convergence with diminishing returns for both A-FADMM and D-FADMM. Our choice $\rho = 0.5$ in Sec. 5 is thus a value yielding sufficiently fast convergence.

In image classification, on the other hand, Fig. 5(b) shows that a smaller ρ is slower at the beginning, but reaches the highest test accuracy faster. For small ρ , the penalty of disagreeing with other workers is not large. Therefore, every worker is likely to be biased towards its local optima. Since each worker has only a fraction of the global dataset, the convergence speed is fast, but the accuracy cannot outperform the global model averaged across all workers. For large ρ , workers tend to strictly reduce the local model disagreement from the beginning. This yields a faster jump to a high accuracy level at the early phase. However, keeping large ρ slows down the updating step by pushing all workers towards minimizing the disagreement in their model updates at every iteration. Given these observations, our choice $\rho = 0.5$ in Sec. 5 is a value yielding sufficiently fast convergence to the highest accuracy. To obviate the accuracy reduction at the beginning while keeping fast convergence speed, studying time-varying ρ (e.g., decreasing ρ from a large value with the number of iterations) could be an interesting topic for future study.

Impact of the Number of Local Iterations. Our image classification relies on DNNs, and thus cannot be solved in a closed form expression. Instead, at every global iteration k , several local iterations are preformed, updating each local model. Ideally, each worker needs to iterate until convergence before sharing the model update, which may however consume too much time. Alternatively, following the standard FL settings [1–3], we run the local training algorithm (i.e., Adam for A-SFADMM and D-SFADMM and SGD for A-SGD) for a few iterations before uploading each

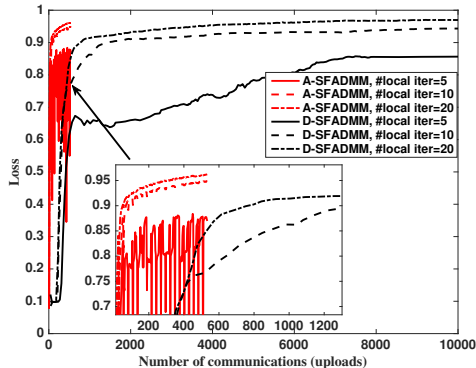


Figure 6: Impact of the *number of local iterations* in image classification using DNNs.

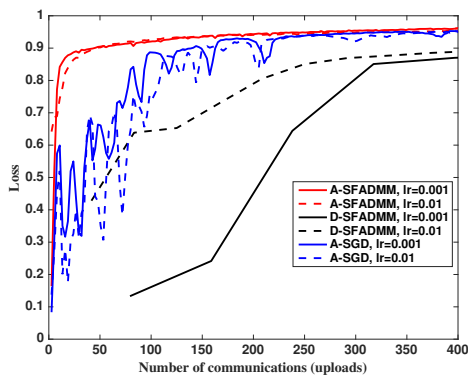


Figure 7: Impact of the *learning rate* in image classification using DNNs.

model. The number of local iterations is critical in ensuring convergence and achieving high accuracy. As shown in Fig. 6, with 5 local iterations both A-SFADMM and D-SFADMM suffer from low accuracy, while A-FADMM even struggles with oscillation. With 20 local iterations, we observe that both A-SFADMM and D-SFADMM achieve not only convergence but also the highest accuracy. Optimizing the number of local iterations is intertwined with learning rate, mini-batch size, and communication channels. This interesting-but-challenging problem is deferred to future work.

Impact of Learning Rates. In Sec. 5, we use the local optimizer’s (Adam or SGD) learning rate 0.01. Here, we additionally test the learning rate 0.001 under $\rho = 5$. As shown in Fig. 7, for A-SFADMM, the learning rate change does not affect the convergence speed and accuracy significantly. By contrast, for D-SFADMM, the learning rate 0.01 leads to faster convergence, while for A-SGD, the learning rate 0.001 yields less oscillation.